Marine Geology 430 (2020) 106368

Contents lists available at ScienceDirect

Marine Geology

journal homepage: www.elsevier.com/locate/margo

Winding down the Chicxulub impact: The transition between impact and normal marine sedimentation near ground zero

Michael T. Whalen [a,*], Sean P.S. Gulick [b,c,d], Christopher M. Lowery [b], Timothy J. Bralower [e], Joanna V. Morgan [f], Kliti Grice [g], Bettina Schaefer [g], Jan Smit [h], Jens Ormö [i], Axel Wittmann [j], David A. Kring [k], Shelby Lyons [e], Steven Goderis [l], and the IODP-ICDP Expedition 364 Scientists [1]

[a] Dept. of Geosciences and Geophysical Institute, University of Alaska Fairbanks, Fairbanks, AK 99775, USA
[b] Institute for Geophysics, Jackson School of Geosciences, University of Texas at Austin, Austin, TX 78758, USA
[c] Department of Geological Sciences, Jackson School of Geosciences, University of Texas at Austin, Austin, TX 79712, USA
[d] Center for Planetary Systems Habitability, University of Texas at Austin, Austin, TX 79712, USA
[e] Department of Geosciences, Pennsylvania State University, University Park, PA 16801, USA
[f] Department of Earth Science and Engineering, Imperial College London, SW7 2AZ London, United Kingdom
[g] Western Australian Organic and Isotope Geochemistry Centre, The Institute for Geoscience Research, School of Earth and Planetary Science, Curtin University, Perth, WA 6102, Australia
[h] Faculty of Earth and Life Sciences (FALW), Vrije Universiteit Amsterdam, 1081 HV Amsterdam, the Netherlands
[i] Centro de Astrobiología Instituto Nacional de Técnica Aeroespacial-Spanish National Research Council (INTA-CSIC), Instituto Nacional de Técnica Aeroespacial, 28850 Torrejon de Ardoz, Spain
[j] Eyring Materials Center, Arizona State University, Tempe, AZ 85287-1704, USA
[k] Lunar and Planetary Institute, Houston, TX 77058, USA
[l] Analytical, Environmental and Geo-Chemistry, Vrije Universiteit Brussel, Brussels, Belgium

ARTICLE INFO

Keywords:
Pelagic sediments
Gulf of Mexico
Tsunami
Seiche
Carbon isotopes

ABSTRACT

The Chicxulub impact led to the formation of a ~ 200-km wide by ~1-km deep crater on México's Yucatán Peninsula. Over a period of hours after the impact the ocean re-entered and covered the impact basin beneath several hundred meters of water. A suite of impactites were deposited across the crater during crater formation, and by the resurge, tsunami and seiche events that followed. International Ocean Discovery Program/International Continental Scientific Drilling Program Expedition 364 drilled into the peak ring of the Chicxulub crater, and recovered ~130 m of impact deposits and a 75-cm thick, fine-grained, carbonate-rich "Transitional Unit", above which normal marine sedimentation resumed. Here, we describe the results of analyses of the uppermost impact breccia (suevite) and the Transitional Unit, which suggests a gradual waning of energy recorded by this local K-Pg boundary sequence.

The dominant depositional motif in the upper suevite and the Transitional Unit is of rapid sedimentation characterized by graded bedding, local cross bedding, and evidence of oscillatory currents. The lower Transitional Unit records the change from deposition of dominantly sand-sized to mainly silt to clay sized material with impact debris that decreases in both grain size and abundance upward. The middle part of the Transitional Unit is interrupted by a 20 cm thick soft sediment slump overlain by graded and oscillatory current cross-laminated beds. The uppermost Transitional Unit is also soft sediment deformed, contains trace fossils, and an increasing abundance of planktic foraminifer and calcareous nannoplankton survivors. The Transitional Unit, as with similar deposits in other marine target impact craters, records the final phases of impact-related sedimentation prior to resumption of normal marine conditions. Petrographic and stable isotopic analyses of carbon from organic matter provide insight into post-impact processes. $\delta^{13}C_{org}$ values are between terrestrial and marine end members with fluctuations of 1–3‰.

Timing of deposition of the Transitional Unit is complicated to ascertain. The repetitive normally graded laminae, both below and above the soft sediment deformed interval, record rapid deposition from currents driven by tsunami and seiches, processes that likely operated for weeks to potentially years post-impact due to

* Corresponding author.
E-mail address: mtwhalen@alaska.edu (M.T. Whalen).
[1] Complete list of expedition scientists is in Appendix A.

https://doi.org/10.1016/j.margeo.2020.106368
Received 7 July 2020; Received in revised form 12 October 2020; Accepted 13 October 2020
Available online 17 October 2020

subsequent continental margin collapse events. Highly siderophile element-enrichment at the top of the unit is likely from fine-grained ejecta that circulated in the atmosphere for several years prior to settling. The Transitional Unit is thus an exquisite record of the final phases of impact-related sedimentation related to one of the most consequential events in Earth history.

1. Introduction

Chicxulub, on the Yucatán Peninsula of México, is one of the best-preserved impact structures on Earth due to its relatively rapid burial by Paleogene carbonate sediments (Fig. 1) (Morgan & Warner, 1999; Whalen et al., 2013). For this reason, the Chicxulub impact structure affords an ideal natural laboratory for documenting cratering events, impact processes, impact melt and breccia deposition, and sedimentary infill of a marine target crater (Gulick et al., 2017; Morgan et al., 2016).

Asteroid or comet impacts into marine target rocks produce a distinctive suite of deposits that are related to crater formation, impact breccia and melt-rock deposition, and resurge of seawater into the crater that reworks and redeposits breccia and melt-rock (Dypvik & Jansa, 2003; Ormö & Lindström, 2000; Wünnemann & Lange, 2002). Of the

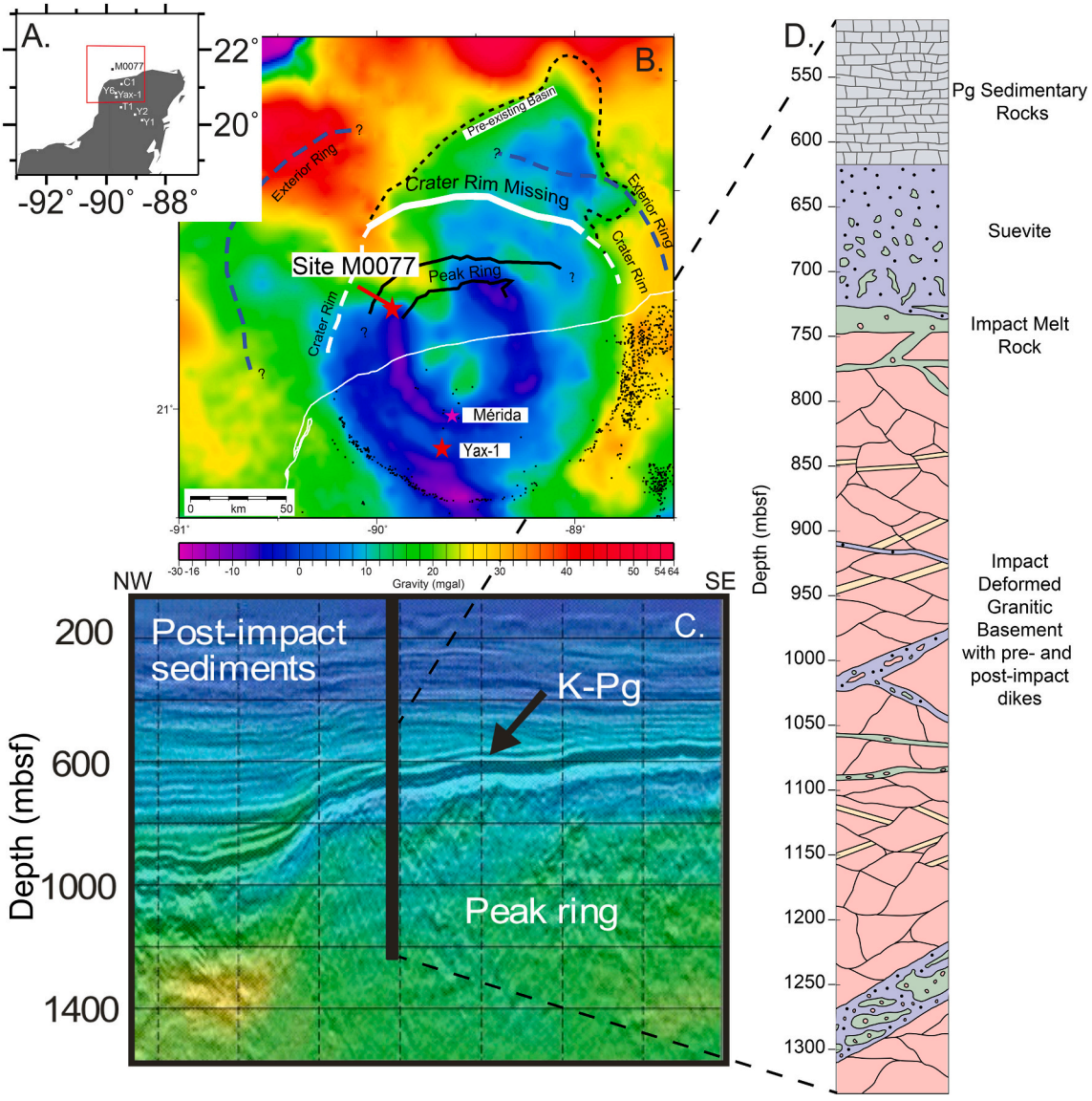

Fig. 1. A) Location of IODP-ICDP Site M0077 in the Gulf of Mexico and other wells illustrated in Fig. 2. The red rectangle indicates the location of B. B) Various crater features like the exterior ring fault (blue dashed line), crater rim (white dashed line), missing crater rim (thick solid white line), and peak ring (solid black line), are illustrated over a Bouguer gravity anomaly map of the Chicxulub impact structure (gravity data courtesy of A. Hildebrand and M. Pilkington). The Yucatán coastline is displayed with the thin white line. Small black dots around southern crater rim indicate cenotes. The location of Site M0077 and Yax-1 are illustrated with red stars. The city of Merida is indicated with a purple star. The position of the seismic line in C is denoted with a red line next to the red star indicating site M0077. Modified from work by Gulick et al. (2008), Christensen et al. (2018), and Lowery et al. (2018). C) Seismic reflection image shown in depth with full waveform velocities overlain. The position of Site M0077 atop the peak ring is illustrated with the crater center toward the southeast. Modified from work by Morgan et al. (2011) and Morgan et al. (2016). D) Lithology documented at Site M0077 from 503.6 m to total depth, illustrating Paleogene sedimentary rocks, suevite, impact melt rock, felsic granitoid basement, suevite and melt rock dikes, and pre- and post-impact dikes. Modified from the work of Morgan et al. (2016). (For interpretation of the references to colour in this figure legend, the reader is referred to the web version of this article.)

previously documented marine impacts, only the Chesapeake Bay impact structure (CBIS; (Dypvik et al., 2018; Gohn et al., 2008; Poag, 1997; Poag, 2002)), Mjølnir (Dypvik et al., 2004), Lockne and Tvären (Frisk & Ormö, 2007; Ormö et al., 2007) have well documented records of this transition from impact-related to normal marine sedimentation. The nearly continuous core-recovery and exceptionally complete record at International Ocean Discovery Program/International Continental Scientific Drilling Program (IODP-ICDP) Site M0077 on the peak ring (an uplifted ring of mountains surrounding the crater's center) of Chicxulub (Morgan et al., 2017) provides insight into the depositional processes operating as the energy associated with the impact and subsequent seismic and continental margin collapse events waned (Gulick et al., 2019; Poag, 2017; Sanford et al., 2016).

Analysis of marine impact deposits and numerical modeling suggests that oblique impacts and those with varying water depths result in strongly asymmetric resurge (Ormö et al., 2010a; Wünnemann et al., 2007). Impact angle and trajectory for Chicxulub were initially examined using gravity data, where conflicting arguments were made on the position of the buried central peak (Hildebrand et al., 1991) versus a basement feature (Schultz & D'Hondt, 1996). Another study looked into how surficial features of impacts such as position of the peak ring or central uplift are not definitive in terms of tracking impact direction (McDonald et al., 2008). A full 3D model of the impact matched against the crustal structure from joint seismic and gravity data was required to work out the signature of impact direction. These data were summarized in Gulick et al. (2013) and the impact trajectory was convincingly modeled with a clear fit to the data at Chicxulub by Collins et al. (2020). This singular attempt at a full 3D hydrocode model of the impact, that matches with the 3D velocity model from refraction data and joint inversions with the gravity data, supports the conclusion of a steeply-inclined (45–60° from horizontal) impact from the northeast (Collins et al., 2020); this trajectory is now broadly adopted by the greater impact cratering community. Such modeling also suggests that there is a larger volume of sedimentary rock volatilization than at either lower or higher impact angles (Artemieva et al., 2017; Collins et al., 2020).

The pre-impact paleogeography of the Yucatán carbonate ramp deepened from tens of meters water depth in the south-southwest to approximately 2 km in the north-northeast (Collins et al., 2008; Gulick et al., 2008). This slope northward into the Gulf of Mexico likely influenced both impact dynamics (Gulick et al., 2008; Ormö et al., 2020) and the resulting resurge of water into the crater (Gulick et al., 2019). When the water is much deeper on one side of a crater, as with Chicxulub (Fig. 1)(Gulick et al., 2008), modeling shows that the deep water resurge will move across the crater faster and may stop or even reverse the resurge at the rim on the shallow water side (Ormö et al., 2010a). The peak ring of the Chicxulub crater was open to the Gulf of Mexico through a gap in the crater rim to the north-northeast (Fig. 1)(Gulick et al., 2008). The asymmetries in the morphology and structure of the transient and final crater, peak ring relief, and the presence or absence of a crater rim (Christeson et al., 1999; Christeson et al., 2001; Gulick et al., 2008; McDonald et al., 2008) likely had a significant effect on resurge and subsequent erosional and depositional processes (Gulick et al., 2019).

Post-impact depositional processes are highly dependent on the impact-generated water movements that in turn depend on the target water depth (Wünnemann et al., 2007). During impacts in which the water depth is less than the diameter of the impactor, (impactor ~12 km (Collins et al., 2020), water depth < 2 km (Gulick et al., 2008)), part of the transient crater rim develops in the water column while part is within the crust. The upper part of the water column within the transient crater collapses outward forming a rim wave tsunami, while simultaneously the lower part collapses inward and water resurges back into the crater (Ormö et al., 2010a; Wünnemann et al., 2007). If the transient crater is largely symmetrical, resurge from all directions results in the formation of a central plume that collapses, causing radial flows that travel back toward the crater rim (Ormö et al., 2010a; Wünnemann et al., 2007). However, the asymmetry of the Chicxulub crater (i.e. presence or absence of a crater rim, variable peak ring relief, (Gulick et al., 2008)) may have prevented the development of a central water plume.

The lack of a crater rim and deeper water to the north/northeast points toward that direction for initial resurge (Gulick et al., 2008; Gulick et al., 2019). Thus, post-impact movement of water in the semi-enclosed crater and the Gulf of Mexico was particularly susceptible to multiple reflected seiches, i.e. standing waves in a partially enclosed body of water, after the initial resurge and rim wave tsunami. The outward radiating rim wave tsunami would have reflected off the highlands of central México, and perhaps the Gulf coastline, forming a reflected tsunami within the first day after impact (Gulick et al., 2019). Waning rim wave energy combined with seismic energy would have created a long-lasting series of seiches moving back and forth across the basin as energy subsided. Deposits as far away as the Adriatic carbonate platform in Croatia appear to record tsunami deposits at the K-Pg boundary (Korbar et al., 2015). Seismic energy may have resulted in a phenomenal inland seiche wave that inundated the Western Interior Seaway, recently documented in a deposit in North Dakota that preserves fossil fish with impact spherules within their gills, an ejecta deposit, and an Ir anomaly (DePalma et al., 2019). Additionally, seismic energy, estimated between M10 (Kring, 1993) and M11 (Day & Maslin, 2005), from the impact induced continental margin collapse and high energy deposits like turbidites, slumps, and slides, around the Gulf resulting in additional tsunami and seiches (Alegret et al., 2001; Bralower et al., 1998; Campbell et al., 2007; Ferrell et al., 2011; Grajales-Nishimura et al., 2000; Paull et al., 2014; Poag, 2017; Sanford et al., 2016; Smit et al., 1992; Soria et al., 2001; Stinnesbeck et al., 1993; Yancey, 1996; Yancey & Liu, 2013). These impact-induced seismic and margin collapse events around the Gulf of Mexico region resulted in the single largest event deposit documented on Earth (Denne et al., 2013; Poag, 2017; Sanford et al., 2016; Scott et al., 2014) and likely influenced deposition within the crater as tsunami and seiche waves entered and moved across the impact basin. Local collapse events from the peak ring itself and the crater rim to the east, south, and west that exhibited 500–800 m of relief (Gulick et al., 2008) could also have resulted in tsunami and seiches that influenced the impact basin. These events and their seismic energy likely waned within years of the impact, following Oromi's law (Parsons, 2002).

IODP/ICDP Expedition 364 recovered core atop the peak ring in the Chicxulub impact structure at Site M0077 (Morgan et al., 2016; Riller et al., 2018). The core penetrated Paleogene sedimentary rocks, suevite, melt rock, and granitic basement (Fig. 1)(Morgan et al., 2016). Deposition of the suevite (polymict, impact melt-bearing breccia, (Claeys et al., 2003; Shoemaker & Chao, 1961; Stöffler & Grieve, 2007) atop the 500 m-high peak ring largely took place during and subsequent to the resurge in a flooded crater (Gulick et al., 2019). The upper suevite, extending from ~617.3–664.5 m below sea floor (mbsf) in the core, records a remarkable succession of 25 fining upward packages that near the base grade upward from coarse pebble to medium sand-size suevite near the base and transition to medium or fine-sand grading into dominantly clay-sized material toward the top (Gulick et al., 2019). The transition between suevite and basal Paleocene limestones is a series of fining upward carbonate-rich couplets, that contains two intervals with soft sediment-deformation, and records the deposition of fine-grained material post-impact (Gulick et al., 2019). This, mostly laminated *Transitional Unit* (616.58–617.33 mbsf, Unit 1G, (Gulick et al., 2017)) is the focus of our study.

2. Regional setting

IODP/ICDP Site M0077 (21.45° N, 89.95° W) is offshore of the Yucatán Peninsula and was chosen due to its position atop a high-relief portion of the Chicxulub peak ring (Fig. 1) (Gulick et al., 2017; Morgan et al., 2016). The site was selected primarily to test models of peak-ring

formation (Morgan et al., 2016). Seismic images of the location suggested that the K-Pg boundary deposit was located within a depression atop the peak ring that was anticipated to contain a relatively complete succession of impact-related and lowermost Paleocene post-impact rocks, at relatively shallow burial depth (Gulick et al., 2019; Morgan et al., 2017). Cores were collected from 505.7–1334.7 mbsf penetrating approximately 110 m of post-impact, hemipelagic and pelagic sedimentary rocks, ranging from middle Eocene (Ypresian) to basal Paleocene (Danian) in age overlying the Transitional Unit and suevite which by definition were deposited in the earliest Danian (Fig. 1)(Gulick et al., 2019; Lowery et al., 2018; Molina et al., 2006; Morgan et al., 2017; Morgan et al., 2016).

2.1. Stratigraphy

Prior to drilling at Site M0077 the stratigraphy of the Chicxulub impact basin was largely informed by a series of relatively deep (1500–3500 m), discontinuously cored, exploratory wells drilled by Petróleos Mexicanos ("Pemex") between the 1950s–70s (Fig. 2)(Hildebrand et al., 1991; Ward et al., 1995). Pemex wells C1, S1, and Y6 penetrated the Paleogene carbonates and underlying suevite but being near the crater center also penetrated intact melt rock (Hildebrand et al., 1991; Kring & Boynton, 1991; Kring & Boynton, 1992; Sharpton et al., 1996; Ward et al., 1995). These wells provided the first impactite samples that were initially misinterpreted as volcanic rocks (Lopez Ramos, 1975). Lower to Upper Cretaceous rocks were penetrated by Pemex wells T1, Y1, and Y2 and contain a mixture of limestone, dolostone, and anhydrite interpreted to represent shallow-water carbonate platform environments (Fig. 2)(Ward et al., 1995). Upper Cretaceous rocks in these wells are overlain by suevite that is in turn overlain by Paleogene carbonate rocks (Ward et al., 1995).

Another series of short cores (60–700 m), that mainly penetrated impact breccia and overlying Paleogene carbonate rocks, were drilled by Universidad Nacional Autónoma de México (UNAM) in the 1990s (Rebolledo-Vieyra et al., 2000; Urrutia-Fucugauchi et al., 1996). The most recent well in the structure prior to IODP/ICDP 364 was the ICDP core Yaxcopoil-1 (Yax-1) drilled in 2001–2002 (Figs. 1-3)(Stinnesbeck et al., 2004; Urrutia-Fucugauchi et al., 2004; Whalen et al., 2013) These onshore wells and cores provide the basic late Mesozoic-early Cenozoic stratigraphic framework of the Yucatán Peninsula (Figs. 1 and 2).

Along with wells and cores, seismic data provide constraints on the subsurface stratigraphy of the Chicxulub structure (Fig. 1). A 1996 experiment collected 650 km of marine two-dimensional (2D) seismic reflection profiles (Morgan & Warner, 1999; Morgan et al., 1997). These data in conjunction with an additional 1500 km of 2D seismic reflection profiles acquired in 2005 (Gulick et al., 2008; Morgan et al., 2005) provide a wealth of information about the crater's structure and the Cenozoic sedimentary infill of the basin (Bell et al., 2004; Gulick et al., 2013; Whalen et al., 2013). The distinctive seismic signature and physical properties of the suevite and related impact deposits enables mapping of the K-Pg event deposits in the Gulf of Mexico (Christeson et al., 2018; Morgan et al., 2011; Sanford et al., 2016).

At Site M0077 Chicxulub impact-related deposits include ~130 m of melt rock and suevite deposited during or shortly after crater formation; water clearly played a role in the emplacement of the sorted upper suevite (Gulick et al., 2019). As these energetic processes waned the termination of these events appears to be recorded in a 75 cm thick micritic unit that documents the transition from impact-related to normal marine sedimentation atop the peak ring in the Chicxulub crater. Here we present a detailed investigation of stratigraphy, sedimentology and stable organic carbon isotope analyses of the organic fraction of the Transitional Unit and contact intervals of super- and subjacent units at Site M0077 that we integrate with published biostratigraphy, ichnology and rare earth element data to provide insight into the waning deposits of one of the most consequential events in Earth history.

3. Materials and methods

We employed visual core description, along with grain size and petrographic analyses, to characterize the lithology and sedimentary structures in the Transitional Unit at Site M0077. Additionally, we analyzed the stable isotopic composition of bulk organic carbon to gain insight into carbon cycling and sources of organic matter in the Transitional Unit. The morphology of micrite, charcoal content, biomarkers

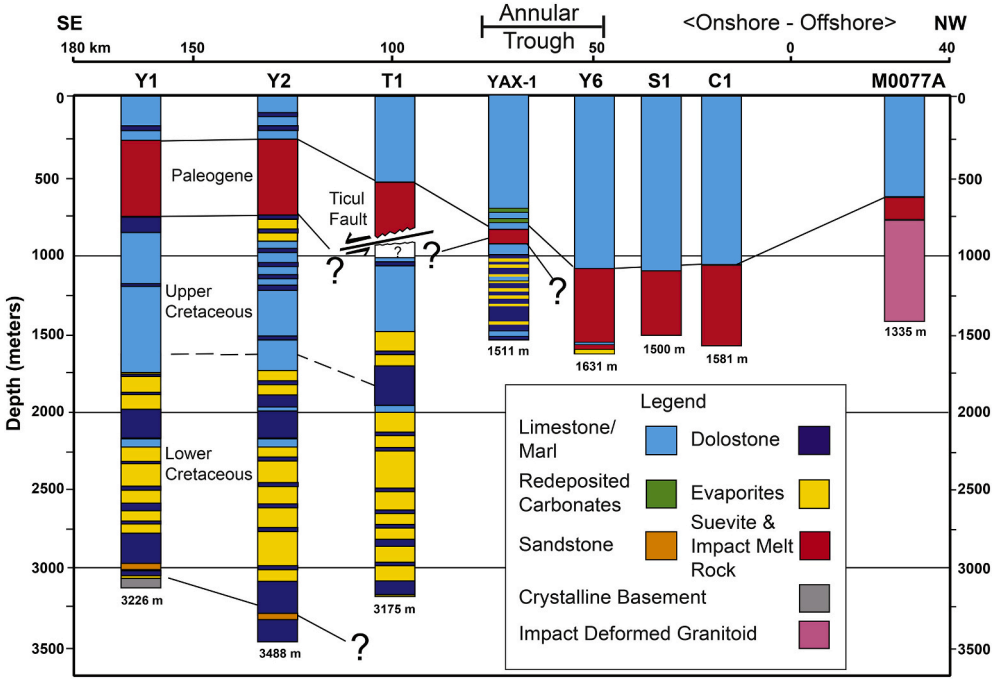

Fig. 2. Generalized regional stratigraphy of the northern Yucatán Peninsula based on subsurface well data. See Fig. 1 for well locations. Modified from work by Ward et al. (1995), Stinnesbeck et al. (2004), Whalen et al. (2013), and Morgan et al. (2017).

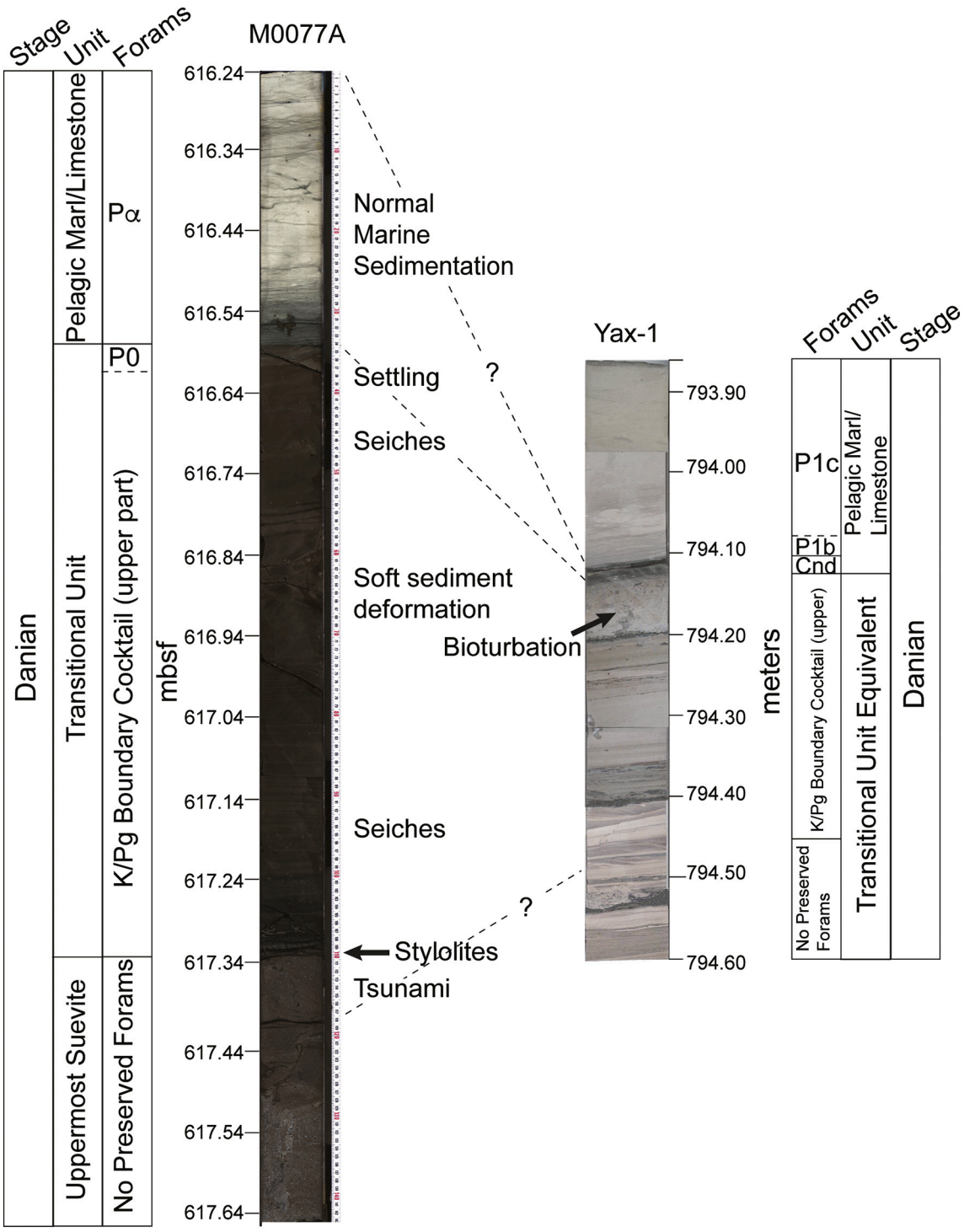

Fig. 3. Stratigraphy of the Transitional Unit and overlying normal marine pelagic Paleocene marlstone and limestone in core from Site M0077 and Yax-1. On the left is a core piece from site M0077 illustrating lithologies between 616.24 and 617.64 mbsf including the uppermost suevite, Transitional Unit, and overlying Paleocene pelagic marlstone and limestone. Note the sharp stylolitized contact (black arrow) at the base of the Transitional Unit (617.33 mbsf). On the right is a core piece from Yax-1 illustrating lithologies between 795.60 and 793.94 m depth including a package correlative with the Transitional Unit at M0077 overlain by a condensed unit (Cnd) and overlying Paleocene rocks. Biostratigraphic data for M0077 are from Morgan et al. (2017) and Lowery et al. (2018), and from Arz et al. (2004) for Yax-1. The K/Pg boundary cocktail includes reworked Cretaceous fossils (Bralower et al., 1998; Lowery et al., 2018). The uppermost portion of the Transitional Unit in both cores records bioturbation in the form of discrete traces at site M0077 (see Fig. 5) and a cross cutting burrow (black arrow) and burrow mottling in Yax-1.

(Bralower et al., 2020a; Bralower et al. (2020b), in press; Gulick et al., 2019; Schaefer et al., 2020), sedimentology, biostratigraphy, and ichnology of the Transitional Unit (Gulick et al., 2017; Lowery et al., 2018; Whalen et al., 2017) are also employed to document the depositional processes associated with the waning energy related to the Chicxulub impact.

3.1. Visual core description

Cores recovered by IODP/ICDP Expedition 364 at Site M0077 were

examined and described by the science party (Morgan et al., 2017) who documented colour, grain size, bedding thickness and character, physical sedimentary structures, fossils, alteration features, and facies stacking patterns. Ichnological analysis focuses on the ichnofabric index (1–5) (Droser & Bottjer, 1986) and the infilling material of the trace fossils (Lowery et al., 2018).

3.2. Grain size analysis

Eleven samples (Table S1) from the Transitional Unit and one from the overlying green marlstone were disaggregated in a bath of hydrogen peroxide or deionized water and were agitated on a shaker table for approximately two weeks. Disaggregated material was decanted to leave behind larger rock fragments that did not break down. The decanted samples were then analyzed using a Beckman Coulter laser diffraction particle size analyzer. Modal, median, and mean grain sizes were obtained (Table S1). We determined D90 values (the grain size fraction that is larger than 90% of all other components in the sample), that were anomalously high thus identifying the coarsest 10% of the total sample. Additional analyses of maximum grain size were determined petrographically as discussed below.

3.3. Thin section petrography

Sixty-three thin sections from the Transitional Unit, 2 from the overlying green marlstone, and 5 from the underlying suevite were examined microscopically under plane and cross polarized light. Transitional Unit samples were categorized using the carbonate classification of Dunham, 1962 as modified by Embry and Klovan, 1972. Bedding, lamination, ichnofabric, and other sedimentary structures were identified. Grains, matrix material and diagenetic products were classified, their mineralogy evaluated, and visible maximum grain diameters for 37 thin sections were measured using the microscope's reticle (Table S2).

3.4. Stable C isotopes

Thirty-eight samples for stable carbon isotope analyses of bulk organic matter ($\delta^{13}C_{org}$)(27 from the Transitional Unit, 4 from the overlying green marlstone, and 7 from underlying upper suevite (Table S3) were prepared by acidifying 1-g subsamples of powdered material with an excess of 1 M HCl. The acid-insoluble residues were rinsed, freeze-dried and analyzed for their C contents using a Costech Elemental Analyzer (ECS 4010). C Isotope ratios were then measured using a Conflo III interface with a Delta+XP Mass Spectrometer and ratios were reported using delta (δ) notation relative to the Vienna PeeDee Belemnite (VPDB). The internal lab standard is peptone No. P-7750 (Sigma Chemical Company, Lot #76f-0300) with $\delta^{13}C = -15.80$. Typical instrumental precision is <0.2‰.

Organic C concentrations in the acid-insoluble residues were used to calculate the whole rock weight percent total organic carbon (TOC) by determining the mass lost during carbonate acidification, also yielding total $CaCO_3$ content (Table S3). The analytical precision and accuracy

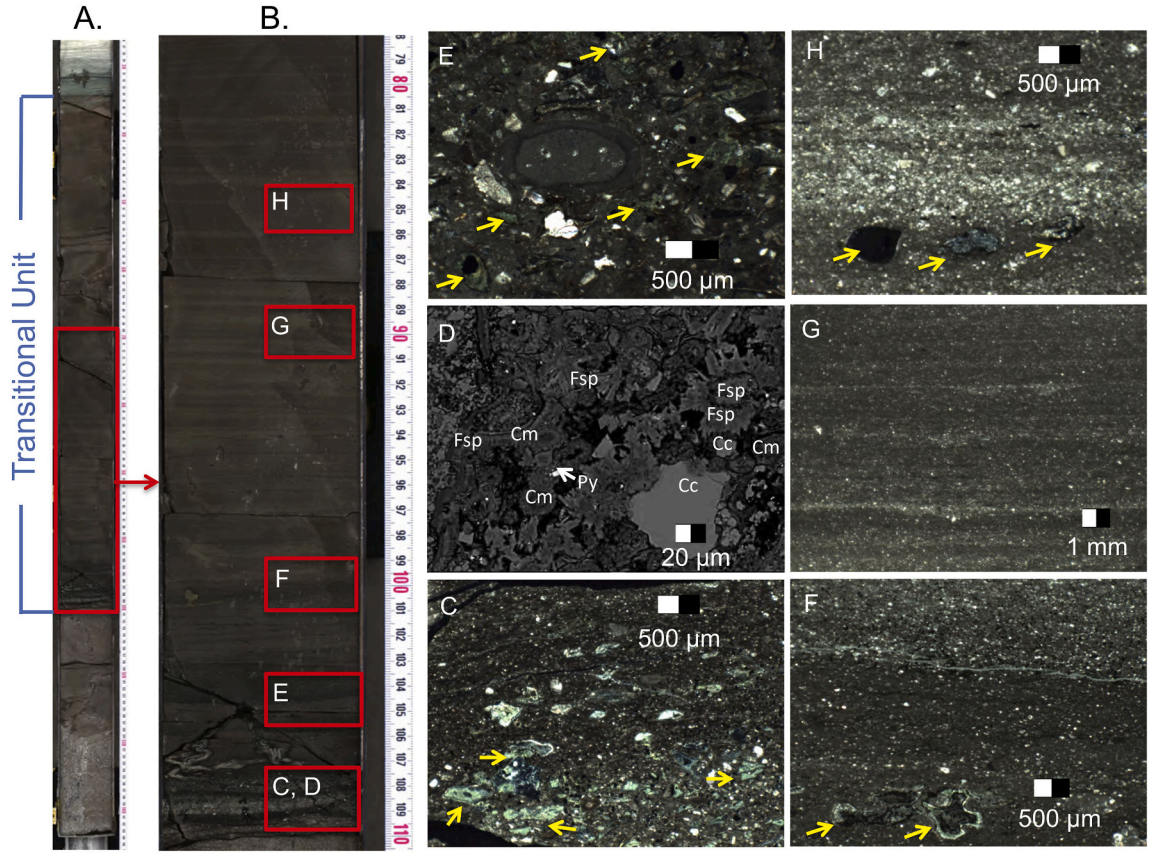

Fig. 4. Lithologies Lower Transitional Unit. A. Core piece 40R-1 illustrating the laminated nature of the Transitional Unit. B. Location of photomicrographs in the lower Transitional Unit. C. Normally graded wackestone with clasts of altered glassy impact melt (yellow arrows) in a micrite matrix. D. Backscattered electron image illustrating the mineralogy of altered impact melt rock fragments. Most alteration products are clay minerals (Cm) or feldspathoids (feldspars or zeolites, Fsp). Also illustrated are crystalline calcite grains (Cc) and pyrite (Py). E. Packstone with bioclasts, crystalline carbonate grains, altered glassy impact melt (yellow arrows) and one large coated carbonate grain near the center of the image. F. Normally graded wackestone with crystalline carbonate grains and altered impact glass (yellow arrows) in a micrite matrix. G. Finely laminated mudstone with thin wackestone to packstone laminae and basal scours. H. Normally graded packstone to wackestone with crystalline and muddy carbonate clasts and altered glassy impact melt (yellow arrows) in a micrite matrix. (For interpretation of the references to colour in this figure legend, the reader is referred to the web version of this article.)

associated with these analyses is respectively within 2% and 5% of the reported values.

4. Results

4.1. Transitional unit: lithology and stratigraphy

The Transitional Unit (Unit 1G, (Gulick et al., 2017)) extends from 616.58–617.33 mbsf (Figs. 3-5), consists dominantly of clay to silt-sized micrite (Table S1)(Bralower et al., 2020b, in press), is underlain by suevite (Unit 2A, (Gulick et al., 2017)) and overlain by green marlstone (Fig. 3)(Unit 1F, (Gulick et al., 2017). The Transitional Unit's lithology is mainly dark brown to dark grayish brown wackestone but the unit is complex with several different lithologies and post-depositional pyrite nodules that disrupt bedding (Figs. 3-5). In general, the Transitional Unit fines upward with a maximum of pebble size grains (up to 4.7 mm) at its base and fine sand size grains (up to 0.20 mm) near its top (Figs. 3-6, Table S2). The unit rests above a cross-bedded package of dominantly sand-sized (up to 2 mm) suevite (Fig. 3)(Gulick et al., 2017; Gulick et al., 2019).

The base of the unit is a sharp, stylolitized contact overlain by two ~1 cm-thick, normally graded beds (617.31–617.33 mbsf) of floatstone, packstone, and wackestone with significant non-carbonate components (Figs. 3, 4). Coarser grains (≤ 4.7 mm) are mainly altered impact glass (clay, zeolite, chalcedony), carbonate intraclasts, composite and coated grains, crystalline calcite grains, foraminifera, and other bioclasts within a micrite matrix (Fig. 4, Table S2). Some grains were altered by the long-lived hydrothermal system in the crater and the peak ring (Kring et al., 2020). Clasts in the basal normally graded beds are similar to those in the underlying suevite. The beds exhibit coarse-tail grading with altered glass and carbonate grains that are locally distributed above similar size grains within a graded bed due to their lower density (Fig. 4A). These two graded beds (617.31–617.33 mbsf) display enrichment of Ni and Cr, based on micro X-ray fluorescence (Fig. 5)(Gulick et al., 2017) and elevated levels of Co, Ir, Ni, Re and Os detected using several analytical methods (Goderis et al., 2019). While this lowermost portion of the Transitional Unit contains altered impact melt rock the bulk of the unit is composed of micrite and is not a polymict conglomerate and thus is not classified as suevite (Claeys et al., 2003; Shoemaker & Chao, 1961; Stöffler & Grieve, 2007).

Above the graded beds (617.01–617.31 mbsf) is a 30 cm thick package of dark gray to dark grayish brown wackestone to mudstone couplets that display submillimeter- to millimeter-scale planar laminations commonly within centimeter-scale beds (Figs. 3-6). Locally laminae are sharp based with erosional scours and have very thin intervals of silt- to sand-sized grains at their base (Fig. 4). Grains are similar to the underlying graded beds but altered impact melt grains become less common and maximum grain size generally decreases upwards (Fig. 6). This package records at least 39, mm to cm-bedded couplets of dark brown and grayish brown wackestone to mudstone with an ichnofabric index of 1 (Fig. 3).

Above this sequence of laminated beds, bedding is indistinct and is obscured by soft sediment deformation from about 616.81–617.01 mbsf (Figs. 3 and 5). Laminae are not present and grains are chaotically arranged (Fig. 5B). Due to soft sediment deformation the ichnofabric index is indeterminate. Truncation of underlying laminae characterizes the base of the deformed unit; the return of bedded facies, similar to those present below the deformation, mark its upper limit (Fig. 3).

Above the deformed interval, in the upper part of the Transitional Unit (616.62–616.81 mbsf), the lowest deposits comprise three cm-scale beds (Figs. 3 and 5). The remainder of this part of the unit is characterized by mm-thick laminae, many with basal erosional scours, low angle cross lamination, and an ichnofabric index of 1 (Fig. 7). Cross laminated intervals commonly display bidirectional laminae and one

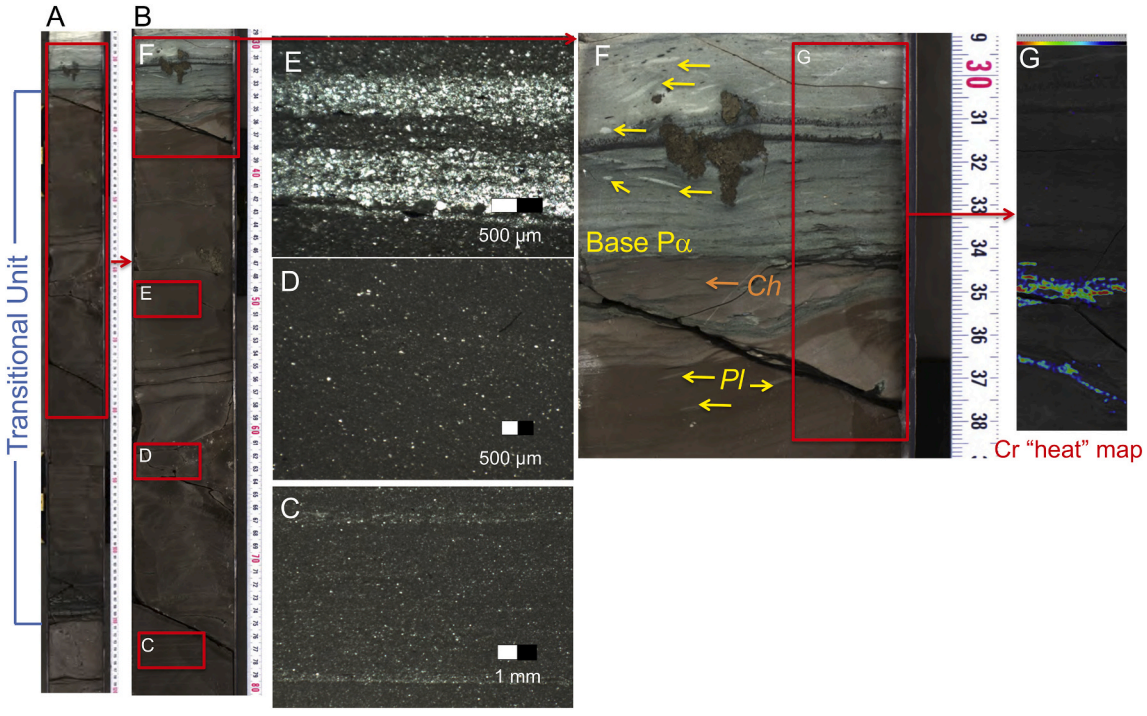

Fig. 5. Lithologies Upper Transitional Unit. A. Core piece 40R-1 illustrating the upper Transitional Unit. B. Location of the position of photomicrographs in the upper Transitional Unit. C. Laminated wackestone with crystalline carbonate grains concentrated at the base of laminae. D. Wackestone within soft-sediment deformed unit. Note the lack of laminae and chaotically arranged crystalline carbonate grains. E. Two normally graded beds overlying the soft-sediment deformed unit indicating resumption of episodically deposited laminae and graded beds. F. Uppermost portion of core 40R-1 illustrating the top of the Transitional Unit and the basal normal-marine Paleocene deposits. The uppermost Transitional Unit contains burrows (yellow arrows = *Planolites*, Pl; orange arrow = *Chondrites*, Ch). The base of the Pα foraminiferal zone is also illustrated. g. X-ray intensity map illustrating relatively high concentrations of Cr at the top of the Transitional Unit (Gulick et al., 2017). (For interpretation of the references to colour in this figure legend, the reader is referred to the web version of this article.)

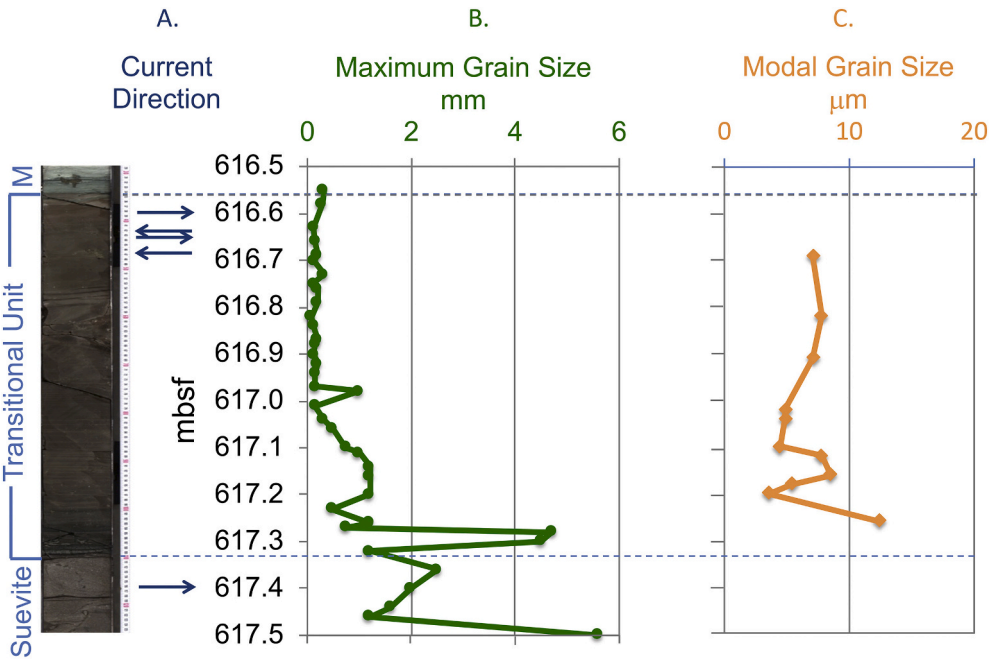

Fig. 6. A. Core section 40R-1 illustrating the uppermost suevite, Transitional Unit, and overlying green marlstone (M). Blue dashed lines indicate unit boundaries. Arrows to the right of the core piece indicate variations in current direction documented from petrographic analyses (see Fig. 7). B. Maximum grain size of the upper most suevite and Transitional Unit based on petrographic thin section analyses (Table S2). C. Modal grain size of the micritic matrix of the Transitional Unit determined with a Beckman Coulter laser diffraction particle size analyzer (Table S1). (For interpretation of the references to colour in this figure legend, the reader is referred to the web version of this article.)

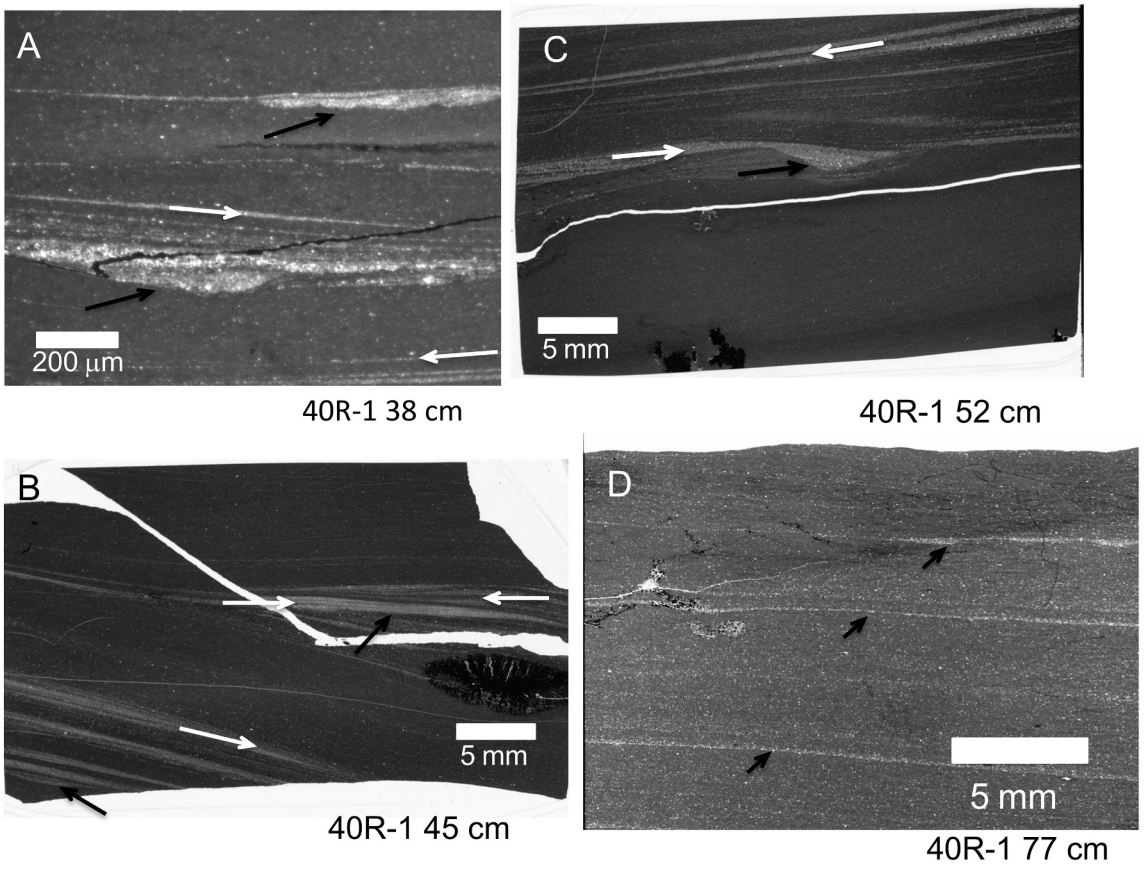

Fig. 7. Photomicrographs illustrating sedimentary structures in the Transitional Unit at Site M0077. White arrows indicate transport direction and black arrows indicate depositional scours. A, B, and C. Wackestone with thin packstone laminae illustrating erosional scours and change in depositional dip of inclined packstone laminae indicating oscillatory flow (616.62, 616.69, 616.76 mbsf respectively). D. Wackestone with thin packstone laminae, each displaying basal erosional scours (617.00 mbsf). All four record an ichnofabric index of 1.

lamina with a well-developed scour (616.77 mbsf), with approximately 2 mm of relief, is overlain by small-scale cross laminae (Fig. 7C). Laminae that offlap and thin in one direction, and then reverse, occur at 616.62, 616.69, and 616.76 mbsf (Fig. 7).

The uppermost part of the Transitional Unit (616.58–616.62 mbsf) is laminated at the mm-scale and the upper 2 cm is a lighter gray-brown colored wackestone and contains a thin interbed of greenish marlstone similar to the overlying unit (Figs. 3 and 5). The strata are slightly deformed with the greenish marlstone and interbedded lighter gray-brown wackestone displaying a distinct down warp and 8 mm of normal-fault displacement from 616.58–616.61 mbsf (Figs. 3 and 5F). The first *Chondrites* and *Planolites* burrows, filled with material similar to the overlying lighter gray-brown micrite, are located at 616.64 mbsf in the darker portion of the uppermost Transitional Unit that has an ichnofabric index of 1 (Fig. 5)(Lowery et al., 2018; Whalen et al., 2017). The lighter colored, uppermost 2 cm of the Transitional Unit is slightly more bioturbated with an ichnofabric index of 2. It contains small *Chondrites* and *Planolites* burrows infilled with material similar to the overlying greenish marlstone, the contact with which (616.58 mbsf) is relatively sharp (Figs. 3 and 5)(Lowery et al., 2018). Charcoal is documented in the uppermost suevite, throughout the Transitional Unit and in the overlying green marlstone, but has spikes in charcoal grain counts in the uppermost suevite and lowermost Transitional Unit (617.24–617.40 mbsf) and the uppermost Transitional Unit (616.58–616.60 mbsf) (Bralower et al., 2020a; Bralower et al. (2020b), in press; Gulick et al., 2019). Above, the overlying greenish marlstone also has an ichnofabric index of 2 and *Chondrites* and *Planolites* burrows (Fig. 5)(Lowery et al., 2018).

4.2. Stable C isotopes - $\delta^{13}C_{org}$ and total organic carbon

Total organic carbon (TOC) values are very low in the Transitional Unit and uppermost suevite, with all samples containing less than 0.15% TOC (Fig. 8, Table S3). $\delta^{13}C_{org}$ values vary between −27.7‰ and −23.4‰ (Fig. 8, Table S3).

In samples from the suevite and the lowermost part of the Transitional Unit $\delta^{13}C_{org}$ values display a monotonic 2.5‰ ^{13}C enrichment (−26.0 to −23.6‰) from 617.26–617.65 mbsf. From that interval up to 616.61 mbsf $\delta^{13}C_{org}$ shows numerous 0.3‰ to 3.8‰ fluctuations with the most ^{13}C-enriched sample (−23.4‰) at 616.79 mbsf and the most ^{13}C-depleted sample (−27.7‰) at 616.73 mbsf. Immediately above that is a positive carbon isotope excursion of 3.8‰ up to 616.61 mbsf. Most of the fluctuations span 4–5 cm of stratigraphy in the core (Fig. 8). Above 616.61 mbsf, to the top of the Transitional Unit and into the lowermost overlying green marlstone, $\delta^{13}C_{org}$ values record a monotonoic negative excursion from −23.9‰ to −26.5‰ (Fig. 8).

5. Discussion

The lithologies in the Transitional Unit represent a continuum of deposition that began with the underlying suevite (Gulick et al., 2019). Understanding the depositional processes of the suevite and the paleogeography of the nascent Chicxulub crater informs our interpretation of deposition of the Transitional Unit. Here we present analysis of the specific features of the Transitional Unit that support its interpretation as the termination of impact-related deposition. We also compare the record at Site M0077 with other proximal localities and the record of post-impact sedimentation in other craters.

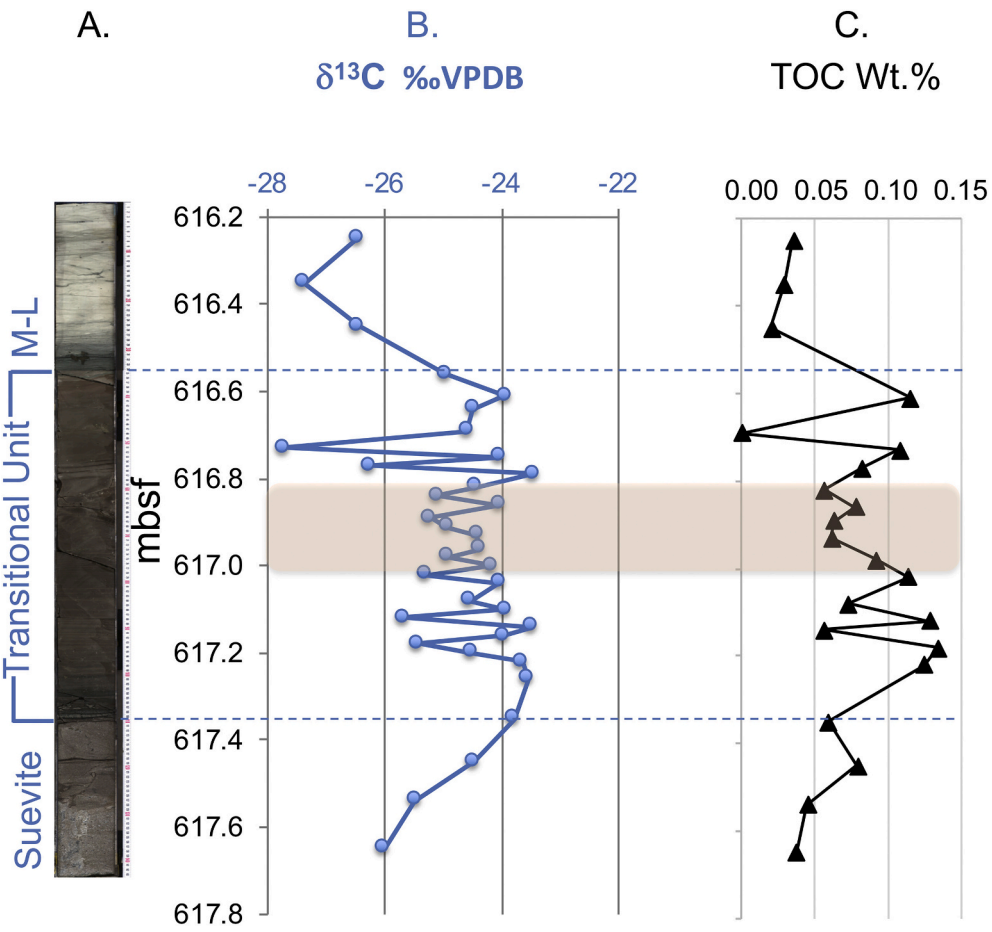

Fig. 8. Stable carbon isotopic and total organic carbon data from samples of the Transitional Unit and adjacent units, Site M0077. A. Core segment 40R-1 illustrating lithologic units including the uppermost suevite, Transitional Unit, and overlying pelagic marlstone and limestone (M-L). Blue dashed lines indicate unit boundaries. B. $\delta^{13}C_{org}$ relative to PDB plotted against mbsf. C. Weight % Total Organic Carbon plotted against mbsf. Shaded interval is soft sediment deformed. (For interpretation of the references to colour in this figure legend, the reader is referred to the web version of this article.)

5.1. Post-impact deposits and processes

Impact events result in probably the most voluminous deposits with the highest accumulation rates of any sedimentological process (Gulick et al., 2019; Sanford et al., 2016). In marine impacts, depending on the relative target water depth, these range from ejecta curtain fallout, processes similar to ground hugging pyroclastic flows, melt-water interactions, marine, debris-, hyperconcentrated-, or suspension flows, avalanches, tsunami and seiches, to long-term post-impact settling of fine material from suspension (Dypvik & Jansa, 2003; Gulick et al., 2019; Ormö et al., 2007; Ormö et al., 2010a; Ormö et al., 2010b; Poag, 2017; Shuvalov et al., 2008). Rocks of the lower suevite (706–721 mbsf) are interpreted to have formed from violent interactions between melt and resurging seawater overlain by deposits from the resurge cresting Site M0077 (698–706 mbsf) (Gulick et al., 2019). In the graded suevite at 698 mbsf, there is a significant change in parameters such as number of clasts per meter, clast size, sorting, roundness, and matrix content (Gulick et al., 2019). Above 698 mbsf, the deposits are interpreted to have formed from settling in the now flooded crater with rapidly decreasing transport energy (Gulick et al., 2019). Above approximately 665 mbsf, the ever-finer grained deposits begin to show repeated graded beds, cross-bedding and other sedimentary structures interpreted as indicating deposition by oscillatory flow, seiches, and local increase in transport energy due to crater-rim generated gravity flows causing seiches within the impact basin (Gulick et al., 2019; Ormö et al., 2020),. This thick package, interpreted as deposits from resurge and settling, is overlain by the cross bedded suevite beginning at 617.42 mbsf (Fig. 3). The Transitional Unit overlies the cross bedded suevite beginning at 617.33 mbsf (Fig. 3)

5.2. Deposition of uppermost suevite and transitional unit

The Transitional Unit records a continued reduction in transport energy that began with the underlying suevite (Gulick et al., 2019) interrupted by episodic increases in energy related to seismic and/or mass wasting events. The upper suevite (617.33–664.52 mbsf, Unit 2A, (Gulick et al., 2017)) at Site M0077 contains about 25 packages that fine upward from gravel to sand sized (35–2 mm) and are interpreted as seiche deposits triggered by earthquakes and submarine slumps, perhaps locally, along the newly formed crater rim or peak ring (Gulick et al., 2019). The uppermost suevite (617.33–617.42 mbsf, Fig. 3) is cross-bedded and interpreted as a deposit from the reflected rim wave tsunami after returning from the Gulf of Mexico shoreline (Gulick et al., 2019). The cross bedded suevite contains terrestrial components including perylene, a polycyclic aromatic hydrocarbon (PAH) that is a pigment made by wood-degrading fungi (Grice et al., 2009), and charcoal, from impact induced fires in terrestrial environments adjacent to the Gulf of Mexico, that were likely transported by tsunami and seiches and deposited in the uppermost suevite and the lowermost Transitional Unit (Bralower et al., 2020a; Bralower et al. (2020b), in press; Gulick et al., 2019).

However, there were also likely additional tsunami and seiche waves that influenced deposition of the Transitional Unit, caused by post-impact seismic and platform margin collapse events in the Gulf of Mexico and Caribbean Sea (Alvarez et al., 1992; Bralower et al., 1998; Denne et al., 2013; Grajales-Nishimura et al., 2009; Kiyokawa et al., 2002; Maurrasse & Sen, 1991; Montanari et al., 1994; Paull et al., 2014; Poag, 2017; Sanford et al., 2016; Tada et al., 2003; Takayama et al., 2000). Soft sediment deformation in the Transitional Unit, reported here, likely attests to continued seismic disturbances and local mass wasting on the topographically high peak ring although site M0077 may have been shielded from some disturbances due to its location in a depression atop the peak ring (Gulick et al., 2019; Morgan et al., 2017). In addition, the crater rim to the east and west was steep (Gulick et al., 2008) and to the south it remained steep for up to 10 Myrs resulting in coarse-grained redeposited carbonates (Whalen et al., 2013) implying that mass wasting and subsequent tsunami and seiches were likely common.

Two relatively coarse-grained, graded beds indicate a change in depositional processes from the underlying cross-bedded suevite to the micrite dominated Transitional Unit that consists predominantly of a series of graded beds (Figs. 3 and 4). Other components in the Transitional Unit include altered glass and grains from sedimentary target rocks (Figs. 4 and 5). The outsized clasts at the base of the initial and subsequent graded beds indicate increased current strength but the range of composition of the clasts (foraminifera, carbonate grains, altered impact glass) complicates determination of current velocity. The general upward decrease in grainsize; however, implies a decrease in current velocity upward. The origin of much of the micrite is likely related to impact processes that vaporized a massive volume of carbonate rock releasing up to 585 Gt of CO_2 (Artemieva et al., 2017). Most of the micrite in the Transitional Unit is interpreted as derived via back-reaction of CaO formed from vaporization of this carbonate (Bralower et al., 2020a) as proposed at other K-Pg boundary sites (Yancey & Guillemette, 2008) although Bralower et al. 2020b, (in press) identified some micrite in the Transitional Unit as microbially precipitated.

Most of the Transitional Unit, above and below the soft sediment deformed interval (616.81–617.01 mbsf), is comprised of laminated and graded beds with basal scours indicating deposition from repeated accelerating and waning currents (Figs. 3-6) which we interpret as deposits from reverberating seiches within the crater. Although basal scours of graded beds represent episodes of increased current agitation, the change from thin graded beds with sand-sized grains in a micrite matrix below the deformed interval to dominantly thin graded beds of silt- to clay-sized carbonate indicates an overall waning of transport energy (Figs. 3-5, and 7).

Currents capable of moving sand to pebble sized grains at similar water depth to Site M0077 are varied and include density currents, deep water tidal currents, benthic storm currents, eddies, internal waves, solitons, and tsunami and seiche related traction currents, among others (Rebesco et al., 2014). Storm currents were considered as a possible transport mechanism but measurements from buoys in the Gulf of Mexico and western Atlantic Ocean demonstrate a maximum of ~250 m for storm wave base (Peters & Loss, 2012). Storm currents would thus seem incapable of moving sediments at the depth of Chicxulub's peak ring (~600 m, (Lowery et al., 2018)). Sand to pebble size grains are transported by the Gulf of Mexico loop current at similar depths along the slope of the modern Campeche Bank (Zavala-Hidalgo et al., 2003). However, the repetitive deposition of graded beds and the occurrence of

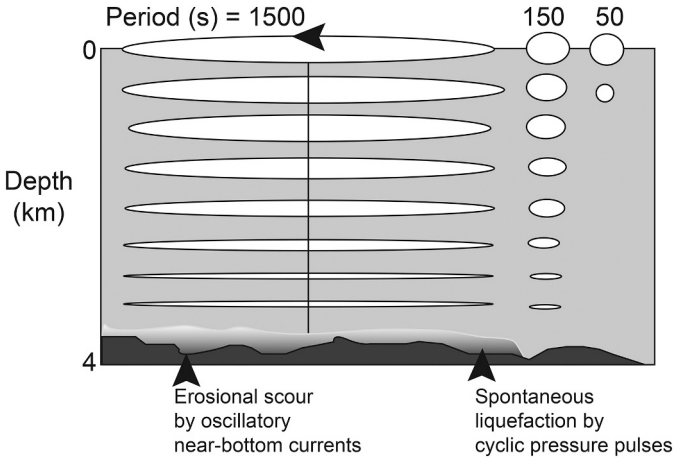

Fig. 9. Conceptual model of tsunami wave passage illustrating the orbital motions created by tsunami of different periods. Vertical displacements are highest at the surface and decrease with depth. Modified from work by Dawson & Stewart (2007).

sedimentary structures indicative of oscillatory flow in the upper Transitional Unit (Figs. 6 and 7) indicate that these were deposited by seiche or tsunami waves. Given their exceptionally long wavelengths (10s–100s of km) tsunami and seiches act as shallow water waves even at abyssal depths (Dawson & Stewart, 2007). Tsunami or seiche waves with periods >3 min can impart oscillatory motion at several km depth (Fig. 9)(Dawson & Stewart, 2007). Based on the physical location within the crater and its proximity to the initial rim wave tsunami, resurge, and mass-wasting derived tsunami and seiches, the latter seems to be the most likely depositional mechanism responsible for most of the sedimentary features recorded in the Transitional Unit.

The period of seiches within the crater, as a semi-enclosed basin, is directly proportional to basin length and inversely proportional to the square root of water depth and can be estimated as being between two end-members:

$T = \frac{2l}{\sqrt{gd}} sec$ for enclosed basins and,

$T = \frac{4l}{\sqrt{gd}}\ sec$ for open basins,

where T = period, l = basin length, g = acceleration of gravity, d = water depth (Trujillo & Thurman, 2017). Given the dimensions of the crater (~180 km diameter, inner rim to inner rim, ~600 m deep peak ring) tsunami or seiche periods of between 78 and 157 min would be expected. Assuming a period in the middle of this range (~100 min) a tsunami wave train and associated seiches within the crater could potentially deposit 25 couplets in about 40 h.

The soft-sediment slump in the middle part of the Transitional Unit (616.81–617.01 mbsf) (Figs. 3 and 5) could be the direct result of seismic shaking or platform-margin collapse and associated tsunami-induced cyclic pressure waves that have the potential to cause spontaneous liquefaction (Fig. 9)(Dawson & Stewart, 2007). Whether related directly to seismicity or platform margin collapse these processes likely waned hyperbolically within years of the impact following Oromi's law (Parsons, 2002). Above the slump, graded bedding and several intervals that clearly indicate oscillatory flow (Figs. 6 and 8) point toward seiches as continued mechanisms of transport and deposition. The smaller-scale soft sediment deformation in the uppermost Transitional Unit (616.58–616.61 mbsf, Fig. 5F) is also significant as it had to occur prior to deposition of the overlying green marlstone. The completely horizontal surface at the top of the Transitional Unit indicates that any topography caused by the deformation was leveled prior to deposition of the green marlstone. This indicates that seismic disturbance and/or slope instability was sustained throughout deposition of most of the Transitional Unit. Processes causing deposition of graded couplets and soft sediment deformation appear to cease and normal marine sedimentation ensued near the top of the Transitional Unit (~616.62 mbsf).

Based on biostratigraphy, He-isotope and Ir analyses the Transitional Unit was likely deposited in months to years at most, with a significant reduction in sedimentation rates in the uppermost few cm (Bralower et al. (2020b), in press; Goderis et al., 2019; Lowery et al., 2018). Microfossils in the Transitional Unit include a mix of reworked Maastrichtian foraminifera and nannofossils (Lowery et al., 2018) commonly referred to as the K-Pg boundary cocktail (Fig. 3)(Bralower et al., 1998). The first well-defined oval structures that are interpreted to be individual *Planolites* and *Chondrites* burrows occur in the upper part of the Transitional Unit (Fig. 5, 616.58–616.65 mbsf) indicating that burrowing organisms were re-established in the crater before the end of deposition of the Transitional Unit (Lowery et al., 2018; Whalen et al., 2017). The settling time, based on Stokes' law, of the fine grained micrite that makes up most of the Transitional Unit suggests that it was deposited in <6 years (Lowery et al., 2018); however, this is a maximum estimate because the sedimentary structures documented here indicate deposition from oscillatory currents. The green marlstone represents 30 kyr post-impact at most, based on biostratigraphy (Lowery et al., 2018) but likely preserves components derived via airfall near its base (Bralower et al. (2020b), in press; Goderis et al., 2019). Specifically, Cr enrichment from μXRF analyses was reported near the top of the Transitional Unit (Fig. 5) (Gulick et al., 2017). Recent trace element analyses identified a 5 cm interval (616.55–616.60 mbsf), spanning the contact of the Transitional Unit with the overlying green marlstone, with significant enrichment in highly siderophile elements, including Ir (Goderis et al., 2019). This enrichment likely indicates deposition of the finest fraction of ejecta which, numerical modeling suggests took approximately 1–5 years to settle from the atmosphere and through the water column (Bardeen et al., 2017; Claeys et al., 2017; Sato et al., 2017; Toon et al., 2016). The presence of charcoal at both the base and top of the Transitional Unit further supports the rapid timeline, wherein the lower charcoal was generated locally by the thermal plume from the impact, whereas the upper charcoal represents fine-grained particles in the stratosphere from globally distributed wildfires (Gulick et al., 2019; Kring & Durda, 2002; Morgan et al., 2013; Wolbach et al., 1990; Bralower et. al., 2020a; Bralower et al., 2020b, in press) and/or soot from heated and ejected fossil organics within the target rocks (Lyons et al., 2020). If we assume deposition of the Transitional Unit took between 3 and 6 years, accumulation rates would be on the order of 25–12.5 cm/yr. These are still extremely high accumulation rates that outpace even those found in glacial settings (Montelli et al., 2017). However, this age information indicates drastic reduction in sedimentation rates post-impact, as rates were as high as 130 m/d while the bulk of the suevite was deposited (Gulick et al., 2019).

5.3. Stable carbon isotopes and total organic carbon

The stable isotopic variations of carbon in organic matter ($\delta^{13}C_{org}$) provides insight into the source(s) of organic matter (transported terrestrial material, microbial mats, and changes in microbial productivity) and biogeochemical carbon cycling within the crater in the immediate and near-term aftermath of the impact event. Total organic carbon contents are uniformly low throughout the Transitional Unit, with a maximum of 0.15 Wt% (Fig. 8). The carbon isotopic data display a rather monotonic positive shift from the uppermost suevite into the lowermost Transitional Unit and in the very uppermost Transitional Unit into the overlying Paleocene facies (Fig. 8). The $^{13}C_{org}$ enrichment in the uppermost suevite and lowermost Transitional Unit (617.26–617.65 mbsf, Fig. 8) coincides with the influx of terrestrially derived material including perylene, charcoal (Bralower et al., 2020a; Bralower et al. (2020b), in press; Gulick et al., 2019) and potentially PAHs, which were also derived from organic matter released from the target rock (Lyons et al., 2020). The upper negative excursion in $\delta^{13}C_{org}$ mirrors that recorded at K-Pg boundary deposits worldwide (Fig. 8)(D'Hondt et al., 1998; Hsü & MacKenzie, 1985; Zachos & Arthur, 1986).

Between 617.2 and 616.7 mbsf, the $\delta^{13}C_{org}$ record displays considerable variation with multiple short-term fluctuations of ~3‰ (Fig. 8). Given the relatively rapid deposition of the Transitional Unit (Bralower et al. (2020b), in press; Lowery et al., 2018) the repeated positive-negative fluctuations in $\delta^{13}C_{org}$ are unlikely associated with extinction-related changes in C (e.g. (Sepúlveda et al., 2019)) but rather variable sediment or organic matter sources. Terrestrial organic matter averages about −22 to −25‰ $\delta\ ^{13}C_{org}$, whereas marine organics can be more negative, approximately −20 to −30‰ (Saltzman & Thomas, 2012). Thus, the positive $\delta^{13}C_{org}$ fluctuations (up to −23.44‰) could be linked to higher concentrations of terrestrial organic matter and the negative values (down to −27.72‰) to relatively higher amounts of marine organics (Fig. 8). We cannot rule out other potential sources of organic carbon, such as ancient terrigenous organic matter eroded from land or carbon released from sedimentary target rocks, which has been identified as a major contributor of PAHs within the Transitional Unit (Lyons et al., 2020). Rather we assume that contemporaneous terrigenous and marine organic matter were dominant source of TOC, as organic matter from the crater was largely burned, ejected, and redistributed globally (Lyons et al., 2020). Evidence of contemporanceous organic matter includes the presence of biomarkers including 2α-

methylhopanes and heterocyst glycolipids in the Transitional Unit that were interpreted as cyanobacterial material from microbial mats transported to the crater by tsunami as well as from blooms of non-heterocystous unicellular pelagic cyanobacteria living in the crater (Schaefer et al., 2020). We suggest that the isotopic shifts are thus likely from a mixing of sources including, but not limited to, terrigenous and marine biomass. The $\delta^{13}C_{org}$ record above the soft sediment deformed interval in the Transitional Unit trends more negatively (Fig. 8), which we interpret as increasing marine input, although additional sources of organics cannot be ruled out.

Recent work by Sepúlveda et al. (2019) examined $\delta^{13}C_{org}$, $\delta^{13}C_{carb}$, $\delta^{13}C_{phytane}$, and $\delta^{15}N_{org}$ from eight neritic to upper bathyal successions in Tunisia, Spain, France and Denmark. They documented spatial and temporal heterogeneity in various carbon isotope records and observe that organic and inorganic carbon are locally decoupled (Sepúlveda et al., 2019). They attributed this heterogeneity to complex processes influencing both organic and inorganic carbon pools. They contend that carbon cycling and primary productivity recovered to pre-K-Pg boundary levels more quickly in these neritic and upper bathyal settings compared to open ocean locations (Sepúlveda et al., 2019) similar to interpretations from microfossils in the Chicxulub crater itself (Lowery et al., 2018). Sepúlveda et al. (2019) also call on productivity driven by non-calcifying phytoplankton analogous to the cyanobacterial productivity interpreted at Site M0077 (Schaefer et al., 2020). Our study provides further evidence for carbon transport and carbon cycle changes as demonstrated by Sepúlveda et al. (2019).

5.4. K-Pg Event deposits and comparison with other gGulf of mMexico records

The K-Pg event deposit, documented at over 350 localities worldwide, varies in stratigraphy with distance from the Chicxulub structure (Schulte et al., 2010; Smit, 1999). Distal deposits (>5000 km from Chicxulub) are very thin (mm-scale), fine-grained, and consist dominantly of platinum group element-enriched clay and spherules and contain shocked quartz and Ni-rich spinels (Schulte et al., 2010; Smit, 1999). Proximal deposits (<1500 km from Chicxulub), on the other hand, are meters to kilometers thick and contain coarse-grained clastic sediments (including suevite), indicating a variety of high-energy depositional processes including resurge, tsunami, seiches, and mass wasting events (Gulick et al., 2019; Poag, 2017; Sanford et al., 2016).

Deposits interpreted as tsunami-derived were a key component in the sedimentology of the K-Pg boundary event (Bourgeois et al., 1988; Smit & Romein, 1985) even before documentation of Chicxulub as the "smoking gun" (Hildebrand et al., 1991). Interpretation of coarse-grained siliciclastic deposits interbedded with shelf mudstones in the Brazos River area (Bourgeois et al., 1988; Smit & Romein, 1985) and other areas (summarized in (Smit, 1999)) were some of the first clues leading to the identification of the Gulf of Mexico region as the potential location of the K-Pg impact (Hildebrand et al., 1991). Several K-Pg outcrop sections along the east coast of México, including La Ceiba, Mimbral, Lajilla, and El Peñon, contain coarse clastic units with local evidence of oscillatory flow that overlie spherule-rich deposits and are interbedded with marls (Smit, 1999). The La Popa basin in northeastern México records a multiphase deposit at the K-Pg boundary with a chaotic, up to 8 m thick, lower portion interpreted as the result of seismicity and shelf collapse, ejecta deposition and reworking by backflow from the initial tsunami. This deposit, with sandstone boulders and abundant shallow water clasts is interpreted as deposited from hyperconcentrated density flows (Schulte et al., 2012). Multiple tsunami backwash deposits characterized by graded beds follow this chaotic unit (Schulte et al., 2012). In Cuba, K-Pg deposits over 500 m-thick contain coarse-grained deposits interpreted as debris flows or turbidites and a finer grained, homogeneous, 40 m-thick unit interpreted as a tsunami deposit (Kiyokawa et al., 2002; Tada et al., 2003; Takayama et al., 2000).

Cores from Deep Sea Drilling Project Sites 536 and 540 in the southeast Gulf of Mexico contain 40 m-thick K-Pg boundary deposits with matrix supported pebbly mudstone overlain by five ~2 m-thick packages of fining upward carbonate sandstone to mudstone with altered impact glass, spherules, and shocked minerals, overlain by about 0.5 m of carbonate mudstone enriched in Ir near the top (Alvarez et al., 1992; Bralower et al., 1998; Sanford et al., 2016). Alvarez et al. (1992) noted that the uppermost fining upward carbonate sandstone to mudstone unit contains bidirectional cross bedding indicating that it was deposited, at least in part, by a tsunami or seiche. Sanford et al. (2016) interpreted the deposit as muddy debris flows overlain by turbidites with the upper 0.5 m recording the settling of fine material suspended by the impact and documented small-scale fining-upward cycles within this package that resemble deposits in the Transitional Unit at Site M0077.

ICDP Yaxcopoil-1 core (Yax-1, Figs. 1, 3), located above Chicxulub's annular trough (Fig. 2), is one of the few other cores that preserves a post-impact succession resting directly atop suevite (Unit 0 of Goto et al. (2004)), Unit 1a of (Stinnesbeck et al. (2004)), that appears to be equivalent to the Transitional Unit at Site M0077. The sorted suevite in Yax-1 is ~29 m thick and contains abundant reworked Cretaceous foraminifers (Arz et al., 2004) and nannofossils and generally fines upward (Goto et al., 2004) as at Site M0077 (Gulick et al., 2019; Ormö et al., 2020). Goto et al. (2004) interpreted the sorted suevite as deposited by resurge. The upper portion of the suevite in Yax-1 (823–795 m) contains 10 normally or inversely graded packages dominated by melt rock fragments but with increasing carbonate lithics up section (Goto et al., 2004). These graded packages are similar to middle portion of the suevite at Site M0077 (Gulick et al., 2017; Gulick et al., 2019). The uppermost suevite (795–798 m) in Yax-1 contains clasts up to 8 mm in diameter (Goto et al., 2004), and is directly overlain by the Transitional Unit equivalent.

The Transitional Unit equivalent in Yax-1 is slightly thinner than at Site M0077 (~50 cm, 794.10–794.64 m, Fig. 3), and comprises a series of normally graded beds near the base, with clasts of altered impact glass, overlain by cross laminated silty to fine sandy dolostone and laminated lime mud-wackestone (Figs. 3 and 10) (Goto et al., 2004; Smit et al., 1992). The cross laminated dolostone (3 units between 794.41 and 794.48 m) locally displays climbing ripple cross lamination (Figs. 3 and 10), interpreted by Goto et al. (2004) as indicating very rapid deposition. This feature was incorrectly identified as "oblique bedding" deposited by weak bottom currents when the structure was described based on an upside-down core piece (Stinnesbeck et al., 2004). Our interpretation departs from that of Stinnesbeck et al. (2004) and Bahlburg et al., 2010 who imply that the fine grain size of the Transitional Unit equivalent in Yax-1 indicates deposition from slowly moving currents. Climbing ripples in Yax-1 (Figs. 3 and 10) argue against this interpretation as they require high rates of suspended load fallout (Jobe et al., 2012). Several intervals record changes in the dip of cross beds indicating oscillatory flow, exemplified by well-developed herringbone cross bedding at 794.56 m (Fig. 10). The occurrence of graded beds, cross-bedding, and multiple levels indicating oscillatory flow in the Transitional Unit equivalent of Yax-1 (Fig. 10) support our interpretation that the unit was deposited by tsunami and seiches and we tentatively correlate the base of the cross beds in Yax-1 with the cross bedded suevite at the top of Unit 2A at Site M0077 (Fig. 3).

5.5. Comparison with other marine impact craters

Comparison of the Transitional Unit at Site M0077 with the uppermost impact-related deposits within other impact structures points toward waning impact and seismic energy as the dominant control on deposition. There are on the order of 15 to 25 known or inferred marine target impact craters documented worldwide (Dypvik & Jansa, 2003; Ormö & Lindström, 2000; Shuvalov et al., 2008). Many of these craters are buried and are known only from geophysical studies or boreholes

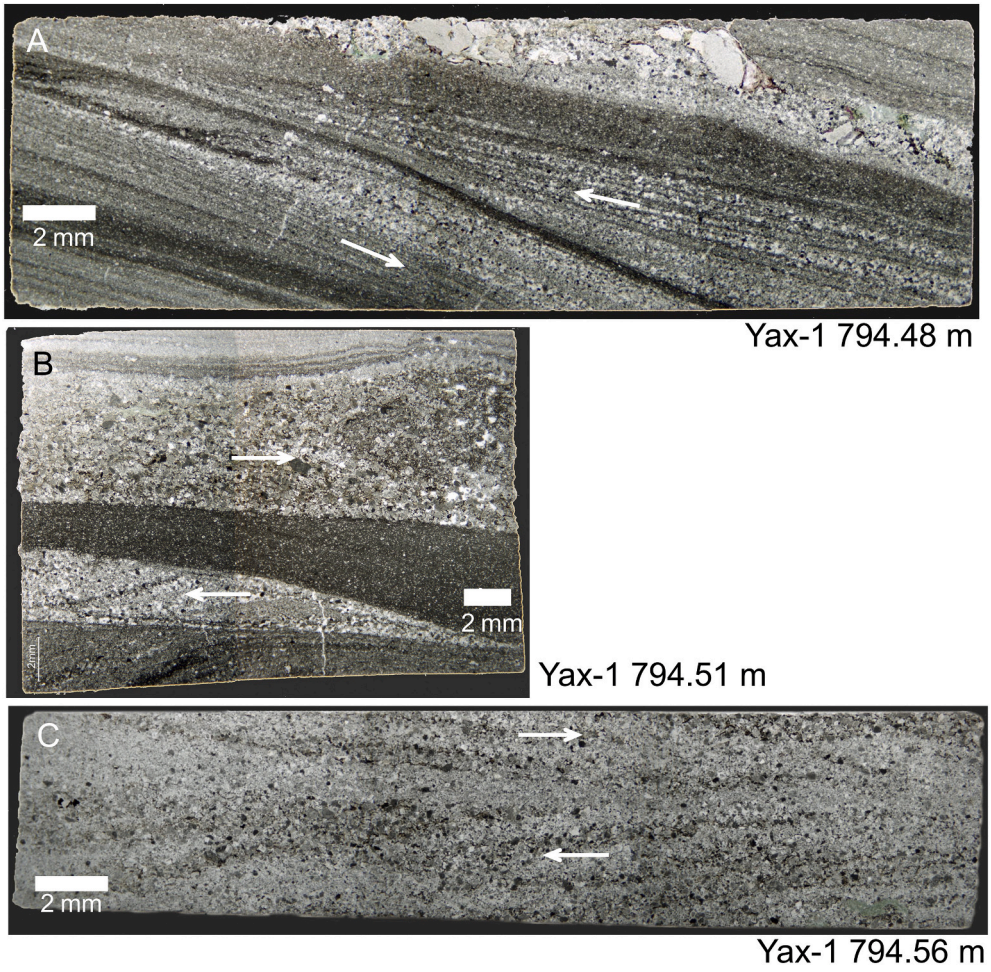

Fig. 10. Photomicrographs illustrating sedimentary structures in the Transitional Unit of Yax-1. White arrows indicate transport direction that alternates, indicating oscillatory flow. A. Fine grained cross-bedded packstone illustrating change in depositional dip of cross laminae within climbing ripples. B. Interbedded dark wackestone and lighter colored coarser-grained packstone illustrating change in depositional dip. C. Packstone displaying herring bone cross bedding.

(Dypvik & Jansa, 2003; Ormö & Lindström, 2000). Of those with cored intervals, only the Chesapeake Bay Impact Structure (CBIS) (Dypvik et al., 2018; Gohn et al., 2008; Poag, 1997; Poag, 2002), and the Mjølnir (Dypvik et al., 2004), Kaluga (Masaitis, 2002), Lockne, and Tvären craters (Frisk & Ormö, 2007; Ormö et al., 2007; Ormö et al., 2010b) have resurge and other post impact deposits sufficiently well documented for direct comparison with the deposits at Site M0077.

The 15-km wide Kaluga crater, located about 150 km south of Moscow, Russia formed in a > 300 m deep Middle Devonian epicontinental sea and is now buried below 800 m of younger strata (Masaitis, 2002). It has been extensively drilled as well as investigated with geophysical methods. Masaitis (2002) describes a complete succession from fractured and brecciated basement, allogenic breccia and suevite, resurge deposits, and post-impact marine sediments. The resurge deposits are approximately 200 m thick and are micrite matrix-supported with up to 5 cm diameter sedimentary and crystalline clasts. The resurge breccia lacks any sign of repeated beds and seems to have been deposited in one single event (Masaitis, 2002) similar to lower suevite at Chicxulub's peak ring (Gulick et al., 2019). Based on a composition dominated by sedimentary clasts it is assumed the material mainly originated from rip-up of the surrounding seafloor, which has also been suggested as the main contributor to the resurge deposits at Tvären, Lockne, and the CBIS (Ormö et al., 2007; Ormö et al., 2009). The Kaluga resurge deposit grades upwards into a claystone, the thickness of which is not reported (Masaitis, 2002).

The Mjølnir impact structure formed in the paleo-Barents sea about 142 Ma and is about 20–40 km across (Dypvik et al., 2004; Werner & Torsvik, 2010). The impact-related stratigraphy documented from a core taken along the slope of the crater's central uplift includes chaotically organized slabs of preimpact sediments, a diamict interpreted as a debris flow, brecciated graded mudstone interpreted to represent tsunami and resurge deposits, and additional debris flow and turbidites prior to resumption of normal marine sedimentation (Dypvik et al., 2004). The breccias are about 14 m thick with multiple fining upward beds (Dypvik et al., 2004). The uppermost meter of the breccia contains conglomerates, parallel and cross laminated sandstones, and matrix and grain supported pebbly mudstone that are interpreted as debris flow or turbidity current deposits (Dypvik et al., 2004). Fossiliferous post-impact sedimentary rocks directly overlie these impact-related rocks and no finer grained counterpart of the Transitional Unit in Chicxulub was documented (Dypvik et al., 2004).

The 7.5 km diameter Lockne (458 Ma) and the 2 km diameter Tvären (460 Ma) impact craters formed within the Ordovician epicontinental Baltoscandian Sea (Lindström and Sturkell, 1992; Ormö et al., 2007; Ormö et al., 2010b). Impactites at Tvären were documented from two drilling sites, whereas Lockne was drilled at 11 locations and most of the impactites are exposed in outcrop. In both craters, impact breccias overlie target rocks and are overlain by a generally fining upward package of polymict gravel to sand-sized breccia grading into siltstones and claystones, the totality interpreted as resurge deposits (Lindström et al., 1994; Ormö et al., 2007; Ormö et al., 2010a; Ormö et al., 2010b). Resurge deposits are up to 125 m thick in Lockne and 70 m thick in

Tvären. The upper part of the resurge succession in both craters is described as a medium-grained to fine-grained arenite (Ormö et al., 2007). At Lockne, this unit may contain up to 20% volume of melt rock fragments, which are interpreted as proximal ejecta that landed in the sea and were transported back into the crater (Lindström et al., 2005). In outcrop on the inner flanks of the crater rim, the lower coarse-grained parts of the resurge arenite commonly show graded beds whereas the upper fine-grained parts display current lineation, cross-bedding, and dewatering structures (Dalwigk & Ormö, 2001). Similar features are seen in the equivalent deposits in drill core from Tvären (Lindström et al., 1994). These deposits appear similar to the upper suevite at Site M0077 in Chicxulub that is cross-bedded with dewatering structures (Gulick et al., 2019). Resurge sands in the cores from Lockne and Tvären fine up into siltstone and silty claystone (up to 32 m thick at Lockne). The contact between the resurge and overlying normal marine facies appears gradual but a sharp boundary was identified chemostratigraphically (Ormö et al., 2010b). The expanded thickness of fine-grained facies at Lockne and Tvären compared to other craters could be a result of the depth of unconsolidated sediment at the time of impact but otherwise the generally fining upward pattern is indicative of a transition from impact related to post-impact sedimentation as we observe at Site M0077.

The CBIS is an 85 km diameter, Late Eocene (ca. 36 Ma) impact structure that is well documented with seismic reflection data and over 15 cored boreholes (Dypvik et al., 2018; Gohn et al., 2008; Poag, 1997; Powars & Bruce, 1999). Water depth at the impact site varied from 0 to 340 m (Horton Jr. et al., 2005). Above crystalline basement, the CBIS impact-related deposits are locally over 1000 m thick and include suevite and lithic breccia, granite slabs, sediment-clast dominated breccia, and a thin stratified member (~1–14 m thick) overlain by post-impact sediments (Dypvik et al., 2018; Gohn et al., 2009; Poag, 1997). The breccias and granite slabs are interpreted as slump deposits. The upper part of the breccia (Exmore Formation, ~425 m in the Eyreville core) contains a basal slump deposit and an upper unit (~87 m) that generally fines upward and is interpreted as a debris flow deposited during resurge (Gohn et al., 2009). The stratified member is broken into two subunits with the lower subunit interpreted as a package of turbidites and the upper subunit as finer-grained turbidites and normal marine suspension deposits (Dypvik et al., 2018; Gohn et al., 2008; Gohn et al., 2009; Poag, 2002).

The succession of impact-related facies in the CBIS shares some interesting features with the deposits recorded at Chicxulub at Site M0077 while also differing significantly. The target rocks of the CBIS, consisting of water-saturated, well indurated Cretaceous and less indurated Paleogene siliciclastic sedimentary rocks overlying Proterozoic and Paleozoic crystalline basement (Gohn et al., 2009; Poag, 1997), differ significantly from the largely carbonate sediments and sedimentary target rocks at Chicxulub. The breccias in the CBIS are highly variable due to a mix of crystalline, consolidated and unconsolidated material involved in the impact (Dypvik et al., 2018; Gohn et al., 2009). The lower stratified interval has sub-horizontal, thick-walled burrows that do not extend into the uppermost stratified interval (Dypvik et al., 2018). The upper stratified member varies between 27 cm and 1.76 m and consists of repetitive submillimeter laminae of very fine to fine sand, silt, and clay (Dypvik et al., 2018; Edwards et al., 2009; Gohn et al., 2009; Poag, 2002). Sand occurs locally as submillimeter to millimeter thick lenses and there are microspherules (< 1 mm diameter) at the base of the laminated unit that are interpreted as fallout ejecta from the impact (Poag, 2002). The upper stratified interval in the CBIS contains no indigenous fauna but impact altered and stratigraphically mixed pre-impact microfossils (Poag, 2002; Poag & Norris, 2005; Self-Trail, 2003). This is similar to the largely reworked nature of Cretaceous foraminifers documented in the Transitional Unit at Site M0077 (Lowery et al., 2018). However, some of these taxa were survivors that became more common in the upper 20 cm of Transitional Unit, prompting Lowery et al. (Lowery et al., 2018) to interpret them as a depauperate survivor fauna that was not reworked.

The upper stratified unit in the CBIS appears to share some characteristics with the Transitional Unit at Site M0077. The laminated sand, silt and clay is reminiscent of the laminae in the Transitional Unit, but at Chicxulub instead of the quartz, mica, and clay observed in the CBIS (Poag, 2002; Poag & Norris, 2005), the laminae comprise altered impact glass, carbonate grains, and micrite. These compositional variations are directly related to the different target rocks at the two different structures but the textural similarity points toward similar depositional processes.

Whereas the stratified unit at the top of the CBIS breccia succession was interpreted as a “dead zone” (Poag, 2002; Poag, 2017; Poag & Norris, 2005), sand filled vertical burrows penetrate into it from the overlying unit (Dypvik et al., 2018). Similarly, *Chondrites* burrows in the uppermost Transitional Unit at site M0077 are filled with material from the overlying green marlstone (Fig. 5). There is additional evidence of life in the form of *Planolites* trace fossils in the upper 20 cm of the Transitional Unit at Site M0077 (Lowery et al., 2018; Whalen et al., 2017). These burrows are flattened and locally infilled with lighter colored overlying micrite that was deposited prior to the first Danian foraminifers indicating the syndepositional nature of the burrows (Lowery et al., 2018). Poag (2002) interpreted the “dead zone” interval as having been deposited from <1 kyr up to 10 kyr post-impact, whereas the Transitional Unit in Chicxulub was likely deposited over the course of several years thus recording a very rapid return of life to the crater (Lowery et al., 2018). A key difference between the two craters is the connection of Chicxulub to the open ocean (Gulick et al., 2008) while the CBIS was at least partially isolated resulting in low oxygen conditions within the post-impact basin that likely delayed the return of life (Dypvik et al., 2018; Poag, 2002).

The above discussion illustrates that the transition from impact-related to post-impact sediment deposition in marine-target craters have some general similarities such as an overall fining upward nature, a transition from sand-sized or coarser-grained impact breccia to laminated fine-grained deposits, and a mix of pre-impact biota, but these impact deposits also vary greatly. The reasons for these variations may be factors such as the relative amount of available water which would affect resurge processes, the morphology of the crater, the location of the core with respect to the crater (e.g. on the rim, in the annular trough, on the peak ring, or in the central crater), the paleogeography of the area (e.g. semi-enclosed basin, open sea), and the general depositional environment (e.g. low vs. high sedimentation rate, energy of the environment).

6. Conclusions

The transition from impact-related to post-impact deposition is recorded in the uppermost cross bedded suevite and a series of graded beds, slumps, and oscillatory flow deposits in the micrite-dominated Transitional Unit at IODP-ICDP Site M0077. This succession shares similarities with other marine-target impact craters including the largely fining upward character of impact breccia with a transition to muddy deposits as the energy from impact-related and seismic events subsided.

The Transitional Unit at Site M0077 thus records the waning of energetic processes initiated by the Chicxulub impact event showing a continuum of deposition with the underlying upper suevite which largely fines upward with dominantly normal and some reverse graded beds. The lower Transitional Unit records at least 39 mm- to cm-scale graded beds with maximum grains of sand size (Figs. 3 and 4). Maximum grain size and inferred velocity generally decrease upward in the Transitional Unit (Fig. 6).

The cross bedded uppermost suevite (Fig. 3) is interpreted as a tsunami deposit while the graded beds in the lower Transitional Unit likely record seiches following this and/or additional tsunami generated by seismic or platform margin collapse events. Influence of terrestrial input in the upper cross bedded suevite and lower Transitional Unit

include perylene, charcoal, and δ $^{13}C_{org}$ values interpreted to represent transported terrigenous organic matter.

Soft sediment deformation in the middle and uppermost portions of the Transitional Unit (Fig. 3) likely indicates either continued seismicity and/or additional tsunami (Fig. 9). Sedimentary structures indicative of scouring are documented throughout the Transitional Unit but the most prominent scour is above the slump interval (Fig. 5) where several beds record evidence of oscillatory flow (Fig. 6) likely generated by seiches.

The uppermost Transitional Unit contains *Planolites* and *Chondrites* burrows (Fig. 5) and elevated numbers of survivor planktic foraminifera and estimates of the timing of deposition indicate a rapid return of life to the crater. Enrichments of highly siderophile elements in the uppermost Transitional Unit and basal overlying green marlstone are interpreted as distal ejecta that likely took several years to settle from the atmosphere and through the water column. This implies that the energy imparted by the impact event and additional water column disturbance related to seismic and platform margin collapse events likely continued for up to several years after the impact but subsided afterwards leading to the resumption of normal marine sedimentation recorded in the overlying Paleocene facies.

The upper suevite, Transitional Unit, and overlying green marlstone on the peak ring of the Chicxulub impact structure at Site M0077 appear to record a complete transition from resurge deposits into post-impact sediments. Several marine-target impact craters record similar successions but the Transitional Unit in Chicxulub appears most similar to the record in the Chesapeake Bay impact structure. This is likely because they are relatively large craters with target materials consisting of water saturated sedimentary rocks overlying crystalline basement. Other craters such as Lockne record a more gradual transition over tens of meters of deposits with tremendous variation depending on location within the crater (Ormö et al., 2009; Ormö et al., 2010a). Thus, we find that the Transitional Unit at Site M0077 records the waning energy related to post-impact seismic and mass-wasting events and the tsunami and seiches these induced eventually giving way to normal marine Paleogene sedimentation. Such a sequence may be indicative of marine impacts.

Declaration of Competing Interest

None.

Data availability

All data are included in the three supplementary tables and the text.

Acknowledgment

The staff at the IODP Core Repository at MARUM, University of Bremen, Germany (especially Holger Kuhlmann) deserve thanks for their help accessing cores and providing follow up samples. We thank Tim Howe, Norma Haubenstock, and Matthew Wooller of the Alaska Stable Isotope Facility for assistance with stable C isotopic analyses and Chris Maio for access and assistance with the Beckman Coulter laser diffraction particle size analyzer. This research was supported by funding from IODP Grant G11100 (Whalen) and National Science Foundation Grants OCE 14-50528 and 1737199 (Whalen), OCE 1736951 (Bralower), OCE 1736826 (Kring), OCE 1737087 (Wittmann), and OCE 1737351 (Gulick and Lowery). An Australian Research Council Grant DP180100982 supported the work of Grice and Schaefer. Work by Goderis was supported by the Belgian Science Policy (BELSPO) and Research Foundation - Flanders (FWO - Vlaanderen). Research by Ormö was partially supported by grants ESP2015-65712-C5-1-R, and ESP2017-87676-C5-1-R from the Spanish Ministry of Economy and Competitiveness and Fondo Europeo de Desarrollo Regional. This is University of Texas Institute for Geophysics Contribution #3710, LPI Contribution #2562, and Center for Planetary Systems Habitability Contribution #0019.

Appendix A. Supplementary data

Supplementary data to this article can be found online at https://doi.org/10.1016/j.margeo.2020.106368.

References

Alegret, L., Molina, E., Thomas, E., 2001. Benthic foraminifera at the cretaceous-tertiary boundary around the Gulf of Mexico. Geology 29, 891–894.

Alvarez, W., Smit, J., Lowrie, W., Asaro, F., Margolis, S.V., Claeys, P., Kastner, M., Hildebrand, A.R., 1992. Proximal impact deposits at the cretaceous-tertiary boundary in the Gulf of Mexico: a restudy of DSDP leg 77 sites 536 and 540. Geology 20, 97–700.

Artemieva, N., Morgan, J., the Expedition 364 Science Party, 2017. Quantifying the release of climate-active gases by large meteorite impacts with a case study of Chicxulub. Geophys. Res. Lett. 44, 1–9. https://doi.org/10.1002/2017GL074879.

Arz, J.A., Alegret, L., Arenillas, I., 2004. Foraminiferal biostratigraphy and paleoenvironmental reconstruction at the Yaxcopoil-1 drill hole (Chicxulub crater, Yucatán Peninsula). Meteorit. Planet. Sci. 39, 1–13.

Bahlburg, H., Weiss, R., Wünnemann, K., 2010. Low energy deposition in the Chicxulub crater during the impact to post-impact transition. Earth Planet. Sci. Lett. 295, 170–176.

Bardeen, C.G., Garcia, R.R., Toon, O.W., Conley, A.J., 2017. On transient climate change at the cretaceous−paleogene boundary due to atmospheric soot injections. Proc. Natl. Acad. Sci. 114, E7415–E7424. www.pnas.org/cgi/doi/10.1073/pnas.1708980114.

Bell, C., Morgan, J.V., Hampson, G.J., Trudgill, B., 2004. Stratigraphic and sedimentological observations from seismic data across the Chicxulub impact basin. Meteorit. Planet. Sci. 39, 1–10.

Bourgeois, J., Hansen, T.A., Wiberg, P. L, and Kauffman, E. G., 1988. A tsunami deposit at the Cretaceous-Tertiary boundary in Texas. Science 241(4865), 567–570.

Bralower, T.J., Paull, C.K., Leckie, R.M., 1998. The Cretaceous-Tertiary boundary cocktail: Chicxulub impact triggers margin collapse and extensive sediment gravity flows. Geology 26, 331–334.

Bralower, T.J., Cosmidis, J., Heaney, P., Kump, L.R., Morgan, J., Harper, D., Lyons, S.L., Freeman, K.H., Grice, K., Wendler, J., Zachos, J.C., Artemieva, N., Gulick, S., House, C., Jones, H.L., Lowery, C.L., Nims, C., Schaefer, B., Si, A., Thomas, E., Vajda, V., 2020a. Origin of a global carbonate layer deposited in the aftermath of the Cretaceous-Paleogene boundary impact. Earth Planet. Sci. Lett. 548, 1–17. https://doi.org/10.1016/J.EPSL.2020.116476.

Bralower, T.J., Cosmidis, J., Fantle, M.S., Lowery, C.L., Passey, B.H., Gulick, S.P.S., Morgan, J.V., Vajda, V., Whalen, M.T., Wittmann, A., Artemieva, N., Farley, K., Goderis, S., Hajek, E., Heaney, P.J., Kring, D.A., Lyons, S.L., Rasmussen, C., Sibert, E., Rodriguez-Tovar, F.J., Turner-Walker, G., Zachos, J.C., Carte, J, Chen, S.A., Cockell, C., Coolen, M., Freeman, K.H., Garber, J., Gonzalez, M., Gray, J.L., Grice, K., Jones, H.L., Schaefer, B, Smit, J. and Tikoo, S.M., 2020b. in press. The habitat of the nascent chicxulub crater, AGU Adv.

Campbell, C.E., Oboh-Ikuenobe, F.E., Eifert, T.L., 2007. Megatsunami deposit in Cretaceous-Paleogene boundary interval of southeastern Missouri. In: Evans, K.R., Horton Jr., J.W., King Jr., D.T., Morrow, J.R. (Eds.), The Sedimentary Record of Meteorite Impacts, 437, pp. 189–198. https://doi.org/10.1130/2008.2437(11). Geological Society of America Special Paper.

Christeson, G.L., Buffler, R.T., Nakamura, Y., 1999. Upper crustal structure of the Chicxulub impact crater from wide-angle ocean bottom seismograph data. In: Dressler, B.O., Sharpton, V.L. (Eds.), Large Meteorite Impacts and Planetary Evolution II, 339, pp. 291–298. Geological Society of America Special Paper.

Christeson, G.L., Nakamura, Y., Buffler, R.T., Morgan, J., Warner, M., 2001. Deep crustal structure of the chicxulub impact crater. J. Geophys. Res. 106, 21,751–21,769. https://doi.org/10.1029/2001JB000337.

Christeson, G.L., Gulick, S.P.S., Morgan, J.V., Gebhardt, C., Kring, D.A., Lebar, E., Lofi, J., Nixon, C., Poelchau, M., Rae, A.S.P., Rebolledo-Vieyra, M., Riller, U., Schmitt, D.R., Wittmann, A., Bralower, T.J., Chenot, E., Claeys, P., Cockell, C.S., Coolen, M.J.L., Ferriere, L., Green, S., Goto, K., Jones, H., Lowery, C.M., Mellett, C., Ocampo-Torres, R., Perez-Cruz, L., Pickersgill, A.E., Rasmussen, C., Sato, H., Smit, J., Tikoo, S. M., Tomioka, N., Urrutia-Fucugauchi, J., Whalen, M.T., Xiao, L., Yamaguchi, K.E., 2018. Extraordinary rocks from the peak ring of the Chicxulub impact crater: P-wave velocity, density, and porosity measurements from IODP/ICDP expedition 364. Earth Planet. Sci. Lett. 495, 1–11. https://doi.org/10.1016/j.epsl.2018.05.013.

Claeys, P., Heuschkel, S., Lounejeva-Baturina, E., Sanchez-Rubio, G., Stöffler, D., 2003. The Suevite of the Chicxulub Impact Crater: Meteoritics and Planetary Science, 38, pp. 1299–1317.

Claeys, P., Goderis, S., de Winter, N.J., Wittmann, A., Whalen, M., the IODP-ICDP Expedition 364 Scientists, 2017. The K/Pg transition on the peak-ring of the Chicxulub impact structure in Core M0077 of IODP-ICDP expedition 364. Lunar Planet. Sci. 1520. XLVIII.

Collins, G.S., Morgan, J., Barton, P., Christeson, G.L., Gulick, S., Urrutia, J., Warner, M., Wünnemann, K., 2008. Dynamic modeling suggests terrace zone asymmetry in the Chicxulub crater is caused by target heterogeneity. Earth Planet. Sci. Lett. 270, 221–230.

Collins, G.S., Patel, N., Davison, T.M., Rae, A.S.P., Morgan, J.V., Gulick, S.P.S., IODP-ICDP Expedition 364 Science Party, 2020. A steeply-inclined trajectory for the

Chicxulub impact. Nat. Commun. 11, 1480. https://doi.org/10.1038/s41467-020-15269-x.
Dalwigk, I., Ormö, J., 2001. Formation of resurge gullies at impacts at sea: the Lockne crater, Sweden. Meteorit. Planet. Sci. 36, 359–370.
Dawson, A.G., Stewart, I., 2007. Tsunami deposits in the geological record. Sediment. Geol. 200, 166–183.
Day, S., Maslin, M., 2005. Linking large impacts, gas hydrates, and carbon isotope excursions through widespread sediment liquefaction and continental slope failure: the example of the K-T boundary event. In: Kenkmann, T., Hörz, F., Deutsch, A. (Eds.), Large Meteorite Impacts III: Geological Society of America Special Paper, 384, pp. 239–258. https://doi.org/10.1130/0-8137-2384-1.239.
Denne, R.A., Scott, E.D., Eickhoff, D.P., Kaiser, J., Hill, R.J., Spaw, J.M., 2013. Massive Cretaceous-Paleogene boundary deposit, deep-water Gulf of Mexico: New evidence for widespread Chicxulub-induced slope failure. Geology 41, 983–986. https://doi.org/10.1130/G34503.1.
DePalma, R.A., Smit, J., Burnham, D.A., Kuiper, K., Manning, P.L., Oleinik, A., Larson, P., Maurrasse, F.J., Vellekoop, J., Richards, M.A., Gurche, L., Alvarez, W., 2019. A seismically induced onshore surge deposit at the KPg boundary, North Dakota. Proc. Natl. Acad. Sci. 116, 8190–8199.
D'Hondt, S., Donaghay, P., Zachos, J.C., Luttenberg, D., Lindinger, M., 1998. Organic carbon fluxes and ecological recovery from the Cretaceous-Tertiary mass extinction. Science 282, 276–279.
Droser, M.L., Bottjer, D.J., 1986. A semiquantitative field classification of ichnofabric. J. Sediment. Petrol. 56, 558–559.
Dunham, R.J., 1962. Classification of carbonate rocks according to depositional texture. In: Hamm, W.E. (Ed.), Classification of Carbonate Rocks—A Symposium, 1, pp. 108–121. American Association of Petroleum Geologists Memoir.
Dypvik, H., Jansa, L.F., 2003. Sedimentary signatures and processes during marine bolide impacts: a review. Sediment. Geol. 161, 309–337.
Dypvik, H., Sandbakken, P.T., Postma, G., Mørk, A., 2004. Early post-impact sedimentation around the central high of the Mjølnir impact crater (Barents Sea, late Jurassic). Sediment. Geol. 168, 227–247.
Dypvik, H., Gohn, G.S., Edwards, L.E., Horton Jr., J.W., Powars, D.S., Litwin, R.J., 2018. Chesapeake Bay Impact Structure—Development of "Brim" Sedimentation in a Multilayered Marine Target. Geol. Soc. Am. Spec. Paper 537, 1–68. https://doi.org/10.1130/2018.2537.
Edwards, L.E., Powars, D.S., Gohn, G.S., Dypvik, H., 2009. Geologic columns for the ICDP-USGS Eyreville A and B cores, Chesapeake Bay impact structure: Sediment-clast breccias, 1096 to 444 m depth. In: Gohn, G.S., Koeberl, C., Miller, K.G., Reimold, W.U. (Eds.), The ICDP-USGS Deep Drilling Project in the Chesapeake Bay Impact Structure: Results from the Eyreville Core Holes, 458. https://doi.org/10.1130/2009.245804. Geological Society of America Special Paper.
Embry III, A.F., Klovan, J.E., 1972. Absolute water depths of late Devonian paleoecological zones. Geol. Rundsch. 61, 672–686.
Ferrell, R., King Jr., D.T., Petruny, L.W., 2011. Nontronitic clay pseudomorphs of Cretaceous-Paleogene (K-T) boundary microtektites, Shell Creek, Alabama, U.S.A. J. Sediment. Res. 81 (5), 348–354. https://doi.org/10.2110/jsr.2011.33.
Frisk, Å., Ormö, J., 2007. Facies distribution of post-impact sediments in the Ordovician Lockne and Tvären impact craters: Indications for unique impact-generated environments. Meteorit. Planet. Sci. 42, 1971–1984.
Goderis, S., Sato, H., Ferrière, L., Schmitz, B., Burney, D., Bralower, T.J., de Graaff, S.J., Dehais, T., de Winter, N.J., Elfman, M., Feignon, J.-G., Gulick, S.P.S., Ishikawa, A., Kaskes, P., Koeberl, C., Kristiansson, P., Lowery, C.M., Morgan, J., Neal, C.R., Owens, J.D., Schulz, T., Sinnesael, M., Smit, J., Vellekoop, J., Whalen, M.T., Wittmann, A., Vanhaeck, F., Van Malderen, S., Claeys, P., 2019. The final settling of meteoritic matter on the peak-ring of the Chicxulub impact structure at Site M0077 of IODP-ICDP Expedition 364. Large Meteorite Impacts Planet. Evol. VI, Abstract #5068, LPI Contrib. No. 2136.
Gohn, G.S., Koeberl, C., Miller, K.G., Reimold, W.U., Browning, J.V., Cockell, C.S., Horton Jr., J.W., Kenkmann, T., Kulpecz, A.A., Powars, D.S., Sanford, W.E., Voytek, M.A., 2008. Deep drilling into the Chesapeake Bay impact structure. Science 320, 1740–1745. https://doi.org/10.1126/science.1158708.
Gohn, G.S., Powars, D.S., Dypvik, H., Edwards, L.E., 2009. Rock avalanche and ocean-resurge deposits in the late Eocene Chesapeake Bay impact structure: Evidence from the ICDP-USGS Eyreville cores, Virginia, USA. In: Gohn, G.S., Koeberl, C., Miller, K.G., Reimold, W.U. (Eds.), The ICDP-USGS Deep Drilling Project in the Chesapeake Bay Impact Structure: Results from the Eyreville Core Holes, 458, pp. 587–615. https://doi.org/10.1130/2009.2458(26). Geological Society of America Special Paper.
Goto, K., Tada, R., Tajika, E., Bralower, T.J., Hasegawa, T., Matsui, T., 2004. Evidence for ocean water invasion into the Chicxulub crater at the cretaceous/Tertiary boundary. Meteorit. Planet. Sci. 39, 1233–1247.
Grajales-Nishimura, J.M., Cedillo Pardo, E., Rosales-Dominguez, C., Moran-Zenteno, D. J., Alvarez, W., Claeys, P., Ruiz-Morales, J., Garcia-Hernandez, J., Padilla-Avila, P., Sanchez-Rios, A., 2000. Chicxulub impact; the origin of reservoir and seal facies in the southeastern México oil fields. Geology 28, 307–310. https://doi.org/10.1130/0091-7613(2000)028<0307:CITOOR>2.3.CO;2.
Grajales-Nishimura, J.M., Murillo-Muneton, G., Rosales-Dominguez, C., Bermudez-Santana, J.C., Velasquillo-Martinez, L.G., Garcia-Hernandez, J., Arz, J.A., Arenillas, I., 2009. The Cretaceous–Paleogene Boundary Chicxulub Impact: Its effect on Carbonate Sedimentation on the Western margin of the Yucatán Platform and nearby areas. In: Bartolini, C., Roman-Ramos, J.R. (Eds.), Petroleum Systems in the Southern Gulf of Mexico, 90. American Association of Petroleum Geologists Memoir, pp. 315–335.
Grice, K., Lu, H., Atahan, P., Asif, M., Hallmann, C., Greenwood, P., Maslen, E., Tulipani, S., Williford, K., Dodson, J., 2009. New insights into the origin of perylene in geological samples. Geochim. Cosmochim. Acta 73, 6531–6543.
Gulick, S., Morgan, J., Mellett, C.L., Green, S.L., Bralower, T., Chenot, E., Christeson, G., Claeys, P., Cockell, C., Coolen, M., Ferriere, L., Gebhardt, C., Goto, K., Jones, H., Kring, D., Lofi, J., Lowery, C., Ocampo-Torres, R., Perez-Cruz, L., Pickersgill, A.E., Poelchau, M., Rae, A., Rasmussen, C., Rebolledo-Vieyra, M., Riller, U., Sato, H., Smit, J., Tikoo, S., Tomioka, N., Urrutia-Fucugauchi, J., Whalen, M., Wittmann, A., Yamaguchi, K., Xiao, L., Zylberman, W., 2017. Site M0077: Post Impact Sedimentary Rocks. the Expedition 364 Scientists, 2017. In: Morgan, J., Gulick, S., Mellett, C.L., Green, S.L. (Eds.), Proceedings of the International Ocean Discovery Program, 364, pp. 1–35. https://doi.org/10.14379/iodp.proc.364.105.2017.
Gulick, S.P.S., Barton, P.J., Christeson, G.L., Morgan, J.V., McDonald, M., Mendoza-Cervantes, K., Pearson, Z.F., Surendra, A., Urrutia-Fucugauchi, J., Vermeesch, P.M., Warner, M.R., 2008. Importance of pre-impact crustal structure for the asymmetry of the Chicxulub impact crater. Nat. Geosci. 1, 131–135.
Gulick, S.P.S., Christeson, G.L., Barton, P.J., Grieve, R.A.F., Morgan, J.V., Urrutia-Fucugauchi, J., 2013. Geophysical characterization of the Chicxulub impact crater. Rev. Geophys. 51, 31–52. https://doi.org/10.1002/rog.20007.
Gulick, S.P.S., Bralower, T.J., Ormö, J., Hall, B., Grice, K., Schaefer, B., Lyons, S., Freeman, K.H., Morgan, J.V., Artemieva, N., Kaskes, P., de Graaff, S.J., Whalen, M. T., Collins, G.S., Tikoo, S.M., Verhagen, C., Christeson, G.L., Claeys, P., Coolen, M.J. L., Goderis, S., Goto, K., Grieve, R.A.F., McCall, N., Osinski, G.R., Rae, A.S.P., Riller, U., Smit, J., Vajada, V., Wittmann, A., and the Expedition 364 Scientists, 2019. Early days of the Cenozoic, Proc. Nat. Acad. Sci. 113, 19342–19351. www.pnas.org/cgi/doi/10.1073/pnas.1909479116.
Hildebrand, A.R., Penfield, G.T., Kring, D.A., Pilkington, M., Camargo, Z.A., Jacobsen, S. B., Boynton, W.V., 1991. Chicxulub Crater: a possible Cretaceous-Tertiary boundary impact crater on the Yucatán Peninsula, México. Geology 19, 867–871.
Horton Jr., J.W., Powars, D.S., Gohn, G.S., 2005. Studies of the ChesapeakeBay impact structure—Introduction and discussion, chap. A. in: Horton, J.W., Jr., Powars, D.S., and Gohn, G.S. (Eds.), Studies of the Chesapeake Bay Impact Structure—the USGS-NASA Langley Corehole, Hampton, Virginia, and Related Coreholes and Geophysical surveys: U.S. Geol. Surv. Prof. Pap. 1688, A1–A24.
Hsü, K.J., MacKenzie, J.A., 1985. A "Strangelove" ocean in the earliest Tertiary. In: Sundquist, E.T., Broecker, W.S. (Eds.), Natural Variations; Archean to Present: American Geophysical Union Geophysical Monograph, 32, pp. 487–492.
Jobe, Z.R., Lowe, D.R., Morris, W.R., 2012. Climbing-ripple successions in turbidite systems: depositional environments, sedimentation rates and accumulation times. Sedimentology 59, 867–898. https://doi.org/10.1111/j.1365-3091.2011.01283.x.
Kiyokawa, S., Tada, R., Iturralde-Vincent, M., Matsui, T., Tajika, E., Tamamoto, S., Oji, T., Nakano, Y., Goto, K., Takayama, H., Garcia Delgado, D., Diaz Otero, C., Rojas Consuegra, R., 2002. Cretaceous-tertiary boundary sequence in the Cacarajicara formation, western Cuba: an impact-related, high-energy, gravity-flow deposit. In: Koeberl, C., MacLeod, K.G. (Eds.), Catastrophic Events and Mass Extinctions: Impacts and Beyond. Boulder, Colorado, Geological Society of America Special Paper, 356, pp. 125–144.
Korbar, T., Montanari, A., Premec, Fucek V., Fucek, L., Coccioni, R., McDonald, I., Claeys, I., Schulz, T., Koeberl, C., 2015. Potential K-Pg tsunami deposits in the intra-Tethyan Adriatic carbonate platform section of Hvar (Croatia). Bull. Geol. Soc. Am. 127, 1666–1680.
Kring, D.A., 1993. The Chicxulub impact event and possible causes of K/T boundary extinctions. In: Boaz, D., Dornan, M. (Eds.), Proceedings of the First Annual Symposium of Fossils in Arizona. Mesa Southwest Museum and Southwest Paleontological Society, Mesa (Arizona), pp. 63–79.
Kring, D.A., Boynton, W.V., 1991. Altered spherules of impact melt and associated relic glass from K/T boundary sediments in Haiti. Geochemica Cosmochimica Acta 55, 1737–1742.
Kring, D.A., Boynton, W.V., 1992. The petrogenesis of an augite-bearing melt rock in the Chicxulub structure and its relationship to K/T impact spherules in Haiti. Nature 358, 141–144.
Kring, D.A., Durda, D.D., 2002. Trajectories and distribution of material ejected from the Chicxulub impact crater: Implications for post-impact widlfires. J. Geophys. Res. 107 https://doi.org/10.1029/2001JE001532, 6–1 – 6-22.
Kring, D.A., Tikoo, S.M., Schmieder, M., Riler, U., Rebolledo-Vieyra, M., Simpson, S.L., Osinski, G.R., Gattacceca, J., Wittmann, A., Verhagen, C.M., Cockell, C.S., Coolen, M. J.L., Longstaffe, F.J., Gulick, S.P.S., Morgan, J.V., Bralower, T.J., Chenot, E., Christeson, G.L., Claeys, P., Ferrière, L., Gebhardt, C., Goto, K., Green, S.L., Jones, H., Lofi, J., Lowery, C.M., Ocampo-Torres, R., Perez-Cruz, L., Pickersgill, A.E., Poelchau, M.H., Rae, A.S.P., Rasmussen, C., Sato, H., Smit, J., Tomioka, N., Urrutia-Fucugauchi, J., Whalen, M.T., Xiao, L., Yamaguchi, K.E., 2020. Probing the hydrothermal system of the Chicxulub Impact Crater. Sci. Adv. 6 https://doi.org/10.1126/sciadv.aaz3053 eaaz3053.
Lindström, M., Sturkell, E.F.F., 1992. Geology of the early Palaeozoic Lockne impact structure, central Sweden. Tectonophysics 216, 169–185.
Lindström, M., Flodén, T., Grahn, Y., Kathol, B., 1994. Post-impact deposits in Tvären, a marine Middle Ordovician crater south of Stockholm, Sweden. Geol. Mag. 131, 91–103.
Lindström, M., Ormö, J., Sturkell, E., von Dalwigk, I., 2005. The Lockne Crater: Revision and reassessment of structure and impact stratigraphy. In: Koeberl, C., Henkel, H. (Eds.), Impact Tectonics Impact Studies. Springer-Verlag, Berlin, pp. 357–388.
Lopez Ramos, E., 1975. Geological summary of the Yucatán Peninsula. In: Nairn, A.E.M., Stehli, F.G. (Eds.), The Ocean Basins and Margins 3, pp. 257–282. The Gulf of Mexico and the Caribbean. New York, Plenum.
Lowery, C.M., Bralower, T.J., Owens, J.D., Rodriquez-Tovar, F.J., Jones, H., Smit, J., Whalen, M.T., Claeys, P., Farley, K., Gulick, S.P.S., Morgan, J.V., Green, S.,

Chenot, E., Christeson, G.L., Cockell, C.S., Coolen, M.J.L., Ferrière, L., Gebhardt, C., Goto, K., Kring, D.A., Lofi, J., Ocampo-Torres, R., Perez-Cruz, L., Pickersgill, A.E., Poelchau, M.H., Rae, A.S.P., Rasmussen, C., Rebolledo-Vieyra, M., Riller, U., Sato, H., Tikoo, S.M., Tomioka, N., Urrutia-Fucugauchi, J., Vellekoop, J., Wittmann, A., Xiao, L., Yamaguchi, K.E., Zylberman, W., 2018. Rapid recovery of life at ground zero of the end-cretaceous mass extinction. Nature 558, 288–291. https://doi.org/10.1038/s41586-018-0163-6.

Lyons, S.L., Karp, A.T., Bralower, T., Grice, K., Schaefer, B., Gulick, S.P.S., Morgan, J., Freeman, K.H., 2020. Organic Matter from the Chicxulub Crater Exacerbated the K-Pg Impact Winter. Proc. Natl. Acad. Sci. https://doi.org/10.1073/pnas.2004596117.

Masaitis, V.L., 2002. The Middle Devonian Kaluga Impact Crater (Russia): New Interpretation of Marine Setting: Deep Sea Research Part II Topical Studies in Oceanography, 49, pp. 1157–1169. https://doi.org/10.1016/S0967-0645(01)00142-4.

Maurrasse, F.J.-M.R., Sen, G., 1991. Impacts, tsunamis and the Haitian Cretaceous-Tertiary boundary layer. Science 252, 1690–1693.

McDonald, M.A., Melosh, H.J., Gulick, S.P.S., 2008. Oblique impacts and peak ring position: Venus and Chicxulub. Geophys. Res. Lett. 35, 1–5. https://doi.org/10.1029/2008GL033346.

Molina, E., Alegret, L., Arenillas, I., Arz, J.A., Gallala, N., Hardenbol, J., von Salis, K., Steurbaut, E., Vandenberghe, N., Zaghbib-Turki, D., 2006. The global boundary stratotype section and point for the base of the Danian stage (Paleocene, Paleogene, "Tertiary", Cenozoic) at El Kef, Tunisia — Original definition and revision. Episodes 29, 263–273.

Montanari, A., Claeys, P., Asaro, F., Bermudez, J., Smit, J., 1994. Preliminary stratigraphy and iridium and other geochemical anomalies across the KT boundary in the Bochil Section (Chiapas, southeastern México). In: New developments regarding the K/T event and other catastrophes in Earth history: Lunar and Planetary Institute Contribution, 825, pp. 84–85.

Montelli, A., Gulick, S.P.S., Worthington, L.L., Mix, A., Davies-Walczak, M., Zellers, S.D., Jager, J.M., 2017. Late Quaternary glacial dynamics and sedimentation variability in the Bering Trough, Gulf of Alaska. Geology 45, 251–254. https://doi.org/10.1130/G38836.1.

Morgan, J., Warner, M., Urrutia-Fucugauchi, J., Gulick, S., Christeson, G., Barton, P., Vieyra, Rebolledo, Melosh, J., 2005. Chicxulub crater seismic survey prepares way for future drilling. EOS 86, 325–332.

Morgan, J., Artemieva, N., Goldin, T., 2013. Revisiting wildfires at the K-Pg boundary. J. Geophys. Res. Biogeo. 118, 1–13. https://doi.org/10.1002/2013JG002428.

Morgan, J., Gulick, S., Mellett, C.L., Green, S.L., and the Expedition 364 Scientists, 2017, Proceedings of the International Ocean Discovery Program 364, doi.10.14379/iodp.proc.364.101.2017.

Morgan, J.V., Warner, M.R., 1999. Chicxulub: the third dimension of a multi-ring impact basin. Geology 27, 407–410.

Morgan J.V., Warner, M. R., and the Chicxulub Working Group, 1997. Size and morphology of the Chicxulub impact crater. Nature 390, 472–476.

Morgan, J.V., Warner, M.R., Collins, G.S., Grieve, R.A.F., Christeson, G.L., Gulick, S.P.S., Barton, P.J., 2011. Full waveform tomographic images of the peak ring at the Chicxulub impact crater. J. Geophys. Res. Solid Earth 116 (B6), B06303.

Morgan, J.V., Gulick, S.P.S., Bralower, T., Chenot, E., Christeson, G., Claeys, P., Cockell, C., Collins, G.S., Coolen, M.J.L., Ferrière Gebhardt, C., Goto, K., Jones, H., Kring, D.A., Leber, E., Lofi, J., Long, X., Lowery, C., Mellett, C., Ocampo-Torres, R., Osinski, G.R., Perez-Cruz, L., Pickersgill, A., Poelchau, M., Rae, A., Rasmussen, C., Rebolledo-Vieyra, M., Riller, U., Sato, H., Schmitt, D.R., Smit, J., Tikoo, S., Tomioka, N., Urrutia-Fucugauchi, J., Whalen, M., Wittmann, A., Yamaguchi, K.E., Zylberman, W., 2016. The formation of peak rings in large impact craters. Science 354, 878–882.

Ormö, J., Lindström, M., 2000. When a cosmic impact strikes the sea bed. Geol. Mag. 137, 67–80.

Ormö, J., Sturkell, E., Lindström, M., 2007. Sedimentological analysis of resurge deposits at the Lockne and Tvären craters: Clues to flow dynamics. Meteorit. Planet. Sci. 42, 1929–1943.

Ormö, J., Sturkell, E., Horton Jr., J.W., Powars, D.S., Edwards, L.E., 2009. Comparison of clast frequency and size in the resurge deposits at the Chesapeake Bay impact structure (Eyreville A and Langley cores): Clues to the resurge process. In: Gohn, G. S., Koeberl, C., Miller, K.G., Reimold, W.U. (Eds.), The ICDPUSGS Deep Drilling Project in the Chesapeake Bay Impact Structure: Results from the Eyreville Core Holes: Geological Society of America Special Paper, 458, pp. 617–632. https://doi.org/10.1130/2009.2458(27.

Ormö, J., Lepinnette, A., Sturkell, E., Lindström, M., Housen, K.R., Holsapple, K.E., 2010a. Water resurge at marine-target impact craters analyzed with a combination of low-velocity impact experiments and numerical simulations. In: Gibson, R.L., Reimold, W.U. (Eds.), Large Meteorite Impacts and Planetary Evolution IV, 465, pp. 81–101. https://doi.org/10.1130/2010.2465(06). Geological Society of America Special Paper.

Ormö, J., Gulick, S.P.S, Whalen, M.T., King, D.T., Sturkell, E., Morgan, J., 2020. A method to assess event magnitude and target water depth for marine-target impacts. Part 1: Granulometry of resurge deposits. Europlanet Science Congress 2020 (EPSC2020-923).

Ormö, J., Hill, A., Self-Trail, J.M., 2010b. A chemostratigraphic method to determine the end of impact related sedimentation at marine-target impact craters (Chesapeake Bay, Lockne, Tvären). Meteorit. Planet. Sci. 45, 1206–1224.

Parsons, T., 2002. Global Omori law decay of triggered earthquakes: large aftershocks outside the classical aftershock zone. J. Geophys. Res. 107 (B9), 2199. https://doi.org/10.1029/2001jb000646.

Paull, C.K., Caress, D.W., Gwiazda, R., Urrutia-Fucugauchi, J., Rebolledo-Vieyra, M., Lundsten, E., Anderson, K., Sumner, E.J., 2014. Cretaceous- Paleogene boundary exposed: Campeche Escarpment, Gulf of Mexico. Marine Geol. 357, 392–400 doi.10.1016 /j.margeo.2014.10.002.

Peters, S.E., Loss, D.P., 2012. Storm and fair-weather wave base: a relevant distinction? Geology 40, 511–514. https://doi.org/10.1130/G32791.1.

Poag, C.W., 1997. The Chesapeake Bay bolide impact: a convulsive event in Atlantic Coastal Plain evolution. Sediment. Geol. 108, 45–95.

Poag, C.W., 2002. Synimpact-postimpact transition inside Chesapeake Bay crater. Geology 30, 995–998.

Poag, C.W., 2017. Shaken and stirred: Seismic evidence of Chicxulub impact effects on the West Florida carbonate platform, Gulf of Mexico. Geology 45, 1011–1014.

Poag, C.W., and Norris, R.D., 2005. Stratigraphy and paleoenvironments of early postimpact deposits at the USGS-NASA Langley corehole, Chesapeake Bay impact crater, chapter F. in: Horton, J.W, Powars, D.S., and Gohn, G.S. (Eds.), Studies of the Chesapeake Bay Impact Structure—the USGS-NASA Langley Corehole, Hampton, Virginia, and Related Coreholes and Geophysical surveys. U.S Geol. Surv. Prof. Pap. 1688, pp. F1–F52.

Powars, D.S., Bruce, T.S., 1999. The effects of the Chesapeake Bay impact crater on the geological framework and correlation of hydrogeologic units of the lower York-James Peninsula, Virginia. U.S. Geol. Surv. Professional Pap. 1612 (82 pp).

Rebesco, M., Hernandez-Molina, F.J., Van Rooij, D., Wahlin, A., 2014. Contourites and associated sediments controlled by deep-water circulation processes: State-of-the-art and future considerations. Mar. Geol. 352, 111–154.

Rebolledo-Vieyra, M., Urrutia-Fucugauchi, J., Marin, L.E., Trejo-Garcia, A., Sharpton, V. L., Soler-Arechalde, A.M., 2000. UNAM Scientific Shallow-Drilling program of the Chicxulub Impact Crater. Int. Geol. Rev. 42, 928–940.

Riller, U., Poelchau, M.H., Rae, A.S.P., Schulte, F.M., Collins, G.S., Melosh, H.J., Grieve, R.A.F., Morgan, J.V., Gulick, S.P.S., Lofi, J., Diaw, A., McCall, N., Kring, D.A., the Expedition 364 Science Party, 2018. Rock fluidization during peak ring formation of large impact craters. Nature 562, 511–519. https://doi.org/10.1038/s41586-018-0607-z.

Saltzman, M.R., Thomas, E., 2012. Chapter 11, Carbon isotope stratigraphy. In: Gradstein, F.M., Ogg, J.G., Schmitz, M., Ogg, G. (Eds.), The Geologic Time Scale 2012. Elsevier, pp. 207–232. https://doi.org/10.1016/B978-0-444-59425-9.00001–9.

Sanford, J.C., Snedden, J.W., Gulick, S.P.S., 2016. The Cretaceous-Paleogene boundary deposit in the Gulf of Mexico: Large-scale oceanic basin response to the Chicxulub impact. J. Geophys. Res. Solid Earth 121, 1–22. https://doi.org/10.1002/2015JB012615.

Sato, H., Ishikawa, A., Ferrière, L., Morgan, J.V., Gulick, S.P.S., 2017. Highly siderophile elements and Os isotope signatures in the K-Pg transition of the Chicxulub peak-ring rocks. In: American Geophysical Union Fall Meeting Abstract P33D-2904.

Schaefer, B., Grice, K., Coolen, M.J.L., Summons, R.E., Cui, X., Bauersachs, T., Schwark, L., Böttcher, M.E., Bralower, T.J., Lyons, S., Freeman, K.H., Cockell, C.S., Gulick, S.P.S., Morgan, J.V., Whalen, M.T., Lowery, C.M., Vajda, V., 2020. Microbial life in the nascent Chicxulub Crater. Geology 48, 328–332. https://doi.org/10.1130/G46799.1.

Schulte, P., Alegret, L., Arenillas, I., Arz, J.A., Barton, P.J., Bown, P.R., Bralower, T.J., Christeson, G.L., Claeys, P., Cockell, C.S., Collins, G.S., Deutsch, A., Goldin, T.J., Goto, K., Grajeles-Nishimura, J.M., Grieve, R.A.F., Gulick, S.P.S., Johnson, K.R., Kiessling, W., Koeberl, C., Kring, D.A., MacLeod, K.G., Matsui, T., Melosh, J., Montanari, A., Morgan, J.V., Neal, C.R., Nichols, D.J., Norris, R.D., Pierazzo, E., Ravizza, G., Rebolledo-Vieyra, M., Reimold, W.U., Robin, E., Salge, T., Speijer, R.P., Sweet, A.R., Urrutia-Fucugauchi, J., Vajda, V., Whalen, M.T., Willumsen, P., 2010. The Chicxulub asteroid impact and mass extinction at the Cretaceous-Paleogene Boundary. Science 327, 1214–1218.

Schulte, P., Smit, J., Deutsch, A., Salges, T., Friese, A., Beichel, K., 2012. Tsunami backwash deposits with Chicxulub impact ejecta and dinosaur remains from the Cretaceous–Palaeogene boundary in the La Popa Basin, Mexico. Sedimentology 59, 737–765. https://doi.org/10.1111/j.1365-3091.2011.01274.x.

Schultz, P.H., D'Hondt, S., 1996. Cretaceous-Tertiary (Chicxulub) impact angle and its consequences. Geology 24, 963–967.

Scott, E.D., Denne, R.A., Kaiser, J.S., Eickhoff, D.P., 2014. Impact on sedimentation into the north-central deep-water Gulf of Mexico as a result of the Chicxulub event. Gulf Coast Assoc.Geol. Sci. J. 3, 41–50.

Self-Trail, J.M., 2003. Shock-wave–induced fracturing of calcareous nannofossils from the Chesapeake Bay impact crater. Geology 31, 697–700. https://doi.org/10.1130/G19678.1.

Sepúlveda, J., Alegret, L., Thomas, E., Haddad, E., Cao, C., Summons, R.E., 2019. Stable isotope constraints on marine productivity across the Cretaceous-Paleogene mass extinction. Paleoceanogr. Paleoclimatol. 34, 1195–1217. https://doi.org/10.1029/2018PA003442.

Sharpton, V.L., Marin, L.E., Carney, J.L., Lee, S., Ryder, G., Schuraytz, B.C., Sikora, P., Spudis, P.D., 1996. A model of the Chicxulub impact basin based on evaluation of geophysical data, well logs, and drill core samples. In: Ryder, G., Fastovsky, D.E., Gartner, S. (Eds.), The Cretaceous-Tertiary Event and Other Catastrophes in Earth History, 307, pp. 55–74. https://doi.org/10.1130/SPE307. Geological Society of America Special Paper.

Shoemaker, E.M., Chao, E.C., 1961. New evidence for the impact origin of the Ries Basin, Bavaria, Germany. J. Geophys. Res. 66, 3371–3378.

Shuvalov, V., Trubetskaya, I., Artemieva, N., 2008. Marine target impacts. In: Adushkin, V.V., Nemchinov, I.V. (Eds.), Catastrophic Events Caused by Cosmic Objects. Springer, Berlin, pp. 291–311.

Smit, J., 1999. The global stratigraphy of the Cretaceous-Tertiary boundary impact ejecta. Annu. Rev. Earth Planet. Sci. 27, 75–113. https://doi.org/10.1146/annurev.earth.27.1.75.

Smit, J., Romein, A.J.T., 1985. A sequence of events across the Cretaceous-Tertiary boundary. Earth Planet. Sci. Lett. 74, 155–170.
Smit, J., Montanari, A., Swinburne, N.H.M., Alvarez, W., Hildebrand, A.R., Margolis, S. V., Claeys, P.F., Lowrie, W., Asaro, F., 1992. Tektite-bearing, deep-water clastic unit at the Cretaceous-Tertiary boundary in northeastern México. Geology 20, 99–103.
Soria, A.R., Liesa, C.L., Mata, M.P., Arz, J.A., Alegret, L., Arenillas, I., Melendez, A., 2001. Slumping and a sandbar deposit at the Cretaceous-Tertiary boundary in the El Tecolote section (northeastern México); an impact-induced sediment gravity flow. Geology 3, 231–234. https://doi.org/10.1130/0091-7613(2001)029<0231:SAASDA>2.0.CO;2.
Stinnesbeck, W., Barbarin, J.M., Keller, G., Lopez-Olivia, J.G., Pivnik, D.A., Lyons, J.B., Officer, C.B., Adatte, T., Graup, G., Roccia, R., Robin, E., 1993. Deposition of channel deposits near the Cretaceous-Tertiary boundary in northeastern México; catastrophic or 'normal' sedimentary deposits? Geology 21, 797–800. https://doi.org/10.1130/0091-7613(1993)021<0797:DOCDNT>2.3.CO;2.
Stinnesbeck, W., Keller, G., Adatte, T., Harting, M., Stuben, D., Istrate, G., Kramer, U., 2004. Yaxcopoil-1 and the Chicxulub impact. Int. J. Earth Sci. 93, 1042–1065. https://doi.org/10.1007/s00531-004-0431-6.
Stöffler, D., Grieve, R.A.F., 2007. Impactites, chapter 2.11. In: Fettes, D., Desmons, J. (Eds.), Metamorphic Rocks: A Classification and Glossary of Terms, Recommendations of the International Union of Geological Sciences Subcommission on the Systematics of Metamorphic Rocks: Cambridge. Cambridge University Press, UK, 258 p.
Tada, R., Iturralde-Vinent, M.A., Matsui, T., Tajika, E., Oji, T., Goto, K., Nakano, Y., Takayama, H., Yamamoto, S., Kiyokawa, S., Toyoda, K., García-Delgado, D., Díaz, C., Rojas, R., 2003. K/T boundary deposits in the paleo-western Caribbean basin. In: Bartolini, C., Buffer, R.T., Blickwede, J. (Eds.), The Circum Gulf of Mexico and the Caribbean: Hydrocarbon Habitats, Basin Formation, and Plate Tectonics, American Association of Petroleum Geologists Memoir, 79, pp. 582–604.
Takayama, H., Tada, R., Matsui, T., Iturralde-Vinent, M.A., Oji, T., Tajika, E., Kiyokawa, S., Garcia, D., Okada, H., Hasegawa, T., Toyoda, K., 2000. Origin of the Peñalver Formation in northwestern Cuba and its relation to K/T boundary impact event. Sediment. Geol. 135, 295–320.
Toon, O.B., Bardeen, C., Garcia, R., 2016. Designing global climate and atmospheric chemistry simulations for 1 and 10km diameter asteroid impacts using the properties of ejecta from the K-Pg impact. Atmos. Chem. Phys. 16, 13185–13212.
Trujillo, A.P., Thurman, H.V., 2017. Essentials of Oceanography, 12th ed. Pearson, New York, New York. 624 pp.
Urrutia-Fucugauchi, J., Marin, L., Trejo-Garcia, A., 1996. UNAM Scientific drilling program of Chicxulub impact structure – evidence for a 300 kilometer crater diameter. Geophys. Res. Lett. 23, 1565–1568.
Urrutia-Fucugauchi, J., Morgan, J., Stoffler, D., Claeys, P., 2004. The Chicxulub Scientific Drilling Project. Meteorit. Planet. Sci. 39, 787–790.
Ward, W.C., Keller, G., Stinnesbeck, W., Adatte, T., 1995. Yucatán subsurface stratigraphy: Implications and constraints for the Chicxulub impact. Geology 23, 873–876.
Werner, S.C., Torsvik, T.H., 2010. Downsizing the Mjølnir impact structure, Barents Sea, Norway. Tectonophysics 483, 191–202. https://doi.org/10.1016/j.tecto.2009.08.036.
Whalen, M.T., Gulick, S.S.P., Pearson, Z.F., Norris, R.D., Perez Cruz, L., Urrutia Fucugauchi, J., 2013. Annealing the Chicxulub Impact: Paleogene Yucatàn Carbonate Slope Development in the Chicxulub Impact Basin, México. In: Verwer, K., Playton, T.E., Harris, P.M. (Eds.), Deposits, Architecture and Controls of Carbonate Margin, Slope, and Basin Systems, 105. Society for Sedimentary Geology Special Publication, pp. 282–304.
Whalen, M.T., O'Malley, K.O., Rodriquez-Tovar, F.J., Morgan, J.V., Gulick, S.P.S, Mellett, C.L., and the IODP-ICDP Expedition 364 Science Party, 2017. Facies and ichnofabrics in the Paleocene of Chicxulub: a record of the recovery of life post-impact. Lunar Planet. Sci. Conf. XLVIII, #1348.
Wolbach, W.S., Gilmour, I., Anders, E., 1990. Major wildfires at the cretaceous/Tertiary boundary. In: Sharpton, V.L., Ward, P.D. (Eds.), Global catastrophes in Earth history: Geological Society of America Special Paper, 247, pp. 391–400.
Wünnemann, K., Lange, M.A., 2002. Numerical modeling of impact-induced modifications of the deep-sea floor. Deep-Sea Research II 49, 969–981.
Wünnemann, K., Weiss, R., Hoffman, K., 2007. Characteristics of oceanic impact-induced large water waves—Re-evaluation of the tsunami hazard. Meteorit. Planet. Sci. 42, 1893–1903.
Yancey, T.E., 1996. Stratigraphy and depositional environments of the Cretaceous-Tertiary boundary complex and basal paleocene section, Brazos River, Texas. Gulf Coast Assoc. Geol. Sci. Trans. 46, 433–442.
Yancey, T.E., Guillemette, R.N., 2008. Carbonate accretionary lapilli in distal deposits of the Chicxulub impact event. Geol. Soc. Am. Bull. 120, 1105–1118.
Yancey, T.E., Liu, C., 2013. Impact-induced sediment deposition on an offshore, mud-substrate continental shelf, Cretaceous-Paleogene boundary, Brazos River, Texas, U. S.A. J. Sediment. Res. 83, 354–367. https://doi.org/10.2110/jsr.2013.30.
Zachos, J.C., Arthur, M.A., 1986. Paleoceanography of the cretaceous/ Tertiary boundary event: Inferences from stable isotopic and other data. Paleoceanography 1, 5–26.
Zavala-Hidalgo, J., Morey, S.L., O'Brien, J.J., 2003. Seasonal circulation on the western shelf of the Gulf of Mexico using a high-resolution numerical model. J. Geophys. Res. 108, 3389. https://doi.org/10.1029/2003JC001879.